THE FINITE ELEMENT SOLUTION OF INVERSE PROBLEMS IN SOLID MECHANICS

by

ANDREW DAVID BARBOUR MCCULLOUGH

B.Sc. (Mechanical Engineering), The University of Manitoba, 1993

A THESIS SUBMITTED IN PARTIAL FULFILLMENT OF

THE REQUIREMENTS FOR THE DEGREE OF

MASTERS OF APPLIED SCIENCE

in

THE FACULTY OF GRADUATE STUDIES

Department of Mechanical Engineering

We accept this thesis as conforming
to the required standard

THE UNIVERSITY OF BRITISH COLUMBIA

September 1995

In presenting this thesis in partial fulfilment of the requirements for an advanced degree at the University of British Columbia, I agree that the Library shall make it freely available for reference and study. I further agree that permission for extensive copying of this thesis for scholarly purposes may be granted by the head of my department or by his or her representatives. It is understood that copying or publication of this thesis for financial gain shall not be allowed without my written permission.

Department of Mechanical Engineering

The University of British Columbia
Vancouver, Canada

Date Oct. 4/95

Abstract

This thesis presents numerical procedures for solving inverse parameter identification problems in solid mechanics. These procedures are applied to the detection of subsurface flaws or cracks and to the study of propagating cracks. The procedure for detecting subsurface defects is based on the process of over-specifying the boundary conditions on the exposed surface of the structure, making an initial assessment about the damage, and then, with the use of nonlinear programming techniques, minimizing a residual vector to reach an optimum solution. The residual vector contains unknown system parameters that characterize the internal defect. The finite element method is combined with a sequential quadratic programming algorithm to solve for these unknown parameters. The procedure utilizes finite element substructuring capabilities in order to minimize the processing and solution time for practical problems. The results obtained from the numerical study verify the accuracy of the algorithm.

The finite element method and nonlinear optimization are also used to solve the inverse parameter identification problem of determining the direction a crack will propagate in a heterogeneous planar domain. This procedure involves determining the direction which produces the maximum strain energy release for a given increment of crack growth. The procedure is applied to four fracture cases of increasing complexity: a horizontal through-thickness crack in a finite plate; an inclined through-thickness crack in a finite plate; a crack parallel to a bimaterial interface; and a transverse crack in two fiber-reinforced composite materials. The results of this numerical study coincide with theoretical predictions and experimentally observed crack growth behavior.

Table of Contents

List of Figures

Acknowledgements

I would like to thank my supervisor, Dr. Mohamed Gadala, for his financial and academic support. His wise advise and insightful guidance in many areas have been invaluable to me.

I would like to extend my appreciation to the Natural Sciences and Engineering Research Council for my post-graduate scholarship, without which I would not have attended UBC.

Chapter 1

Introduction

1.1 Background and Literature

1.1.1 Inverse Problems

Internal cracks and flaws may seriously degrade the structural integrity, life expectancy and performance of a structure. As a result, techniques for the early detection of subsurface defects, or for studying the behavior of internal cracks, are of practical importance. The procedures presented in this thesis provide a numerical means for identifying subsurface flaws or cavities and for determining the direction a crack will propagate in a heterogeneous domain. The solution to these problems is based on formulating them in a inverse manner.

An inverse problem is defined as any problem which can not be classified as a direct problem. As described by Kubo [1], a direct problem involves determining the response of a system given the following information; the domain of a problem and its boundaries, governing laws or equations, and the boundary conditions and forcing functions. In practice, this information may not be complete, making a direct analysis of a problem infeasible. However, if additional information, such as a prescribed system response is specified, an inverse problem may be constructed to determine the required input for the direct problem.

In the past decade the study of inverse problems has received increased attention, as

many researchers have begun to recognize their importance in various fields of science and engineering. Early examples of inverse problems can be found in the area of heat transfer, where comprehensive literature reviews are given by Dulikravich [2] and Beck, et al. [3]. Examples of inverse problems also arise in other fields in the form of exploration techniques in geophysics, X-ray computed tomography in medical science, signal recovery in optics, and airfoil design in fluid mechanics. In solid mechanics and structural analysis, examples of inverse problems include shape optimization [4], determination of contact stresses [5,6], and detection of subsurface flaws or cracks [7-14]. Kubo [1] and Bui [15] presented reviews of inverse problems in this field.

The inverse problems considered for this research are referred to as parameter identification problems [5] since they are concerned with determining geometric or material related system parameters. Another class of inverse problems, known as reconstruction problems, are also identified in the field of solid mechanics . These types of problems are concerned with determining response related information, such as contact stresses and boundary tractions.

1.1.2 Subsurface Cavity Detection

Flaw detection for structural components is required for many industrial applications. A variety of nondestructive testing methods, such as Ultrasonics, Radiography, Acoustic Emissions and magnetic techniques, are commonly used for this purpose, but the information they provide is usually limited. In addition, these procedures may not be applicable for inaccessible areas on a specimen. Consequently, a growing interest in the development of

efficient and accurate computational approaches, which formulate the nondestructive inspection or evaluation as an inverse problem, have recently emerged.

The procedure for numerically detecting subsurface flaws is commonly based on characterizing the defect using several geometric and material parameters. These parameters are iteratively modified throughout the inverse analysis until a convergent solution is obtained; at which point, the pre-defined parameters should correctly represent the internal flaw. The system parameters are updated by minimizing a functional using optimization techniques. For subsurface cavity detection, the functional is typically an expression comparing numerically calculated and experimentally determined displacements on the exterior of the structure. A more comprehensive description of this approach is given in Chapter 2.

A variety of numerical methods and optimization techniques are available for updating the parameter set and for calculating the exterior displacements. Tanaka et al. [9] utilized the boundary element method to separately determine the center location and radius of a circular void in a rectangular plate that was subjected to dynamic loading conditions. Tanaka and Masuda [10] used the boundary element method, integral equations, and internal stresses as the reference data to determine the shape of an internal flaw. Kassab et al. [11] also used the boundary element method to simultaneously determine the location and size of a subsurface cavity in a rectangular plate. This solution procedure employed the Newton-Raphson method to update the parameter vector by solving a set of nonlinear equations. The problem of subsurface crack detection was examined by Melling and Aliabad [12]. This research incorporated the constrained Steepest Descent updating technique in conjunction with the boundary element method to predict the position and length of subsurface straight and curved

cracks. Recently, Hsich and Mura [7] used the the Levenberg-Marquardt optimization method, the boundary element technique and internal displacement information to determine the size and location of an elliptical flaw. Schnur and Zabaras [5] utilized the finite element method to calculate exterior displacements on a square plate. A modified Levenberg-Marquardt method was used in to minimize the nonlinear least square function, however, problems were encountered in the convergence of the optimization method when guess values deviated slightly from the true values. For these numerical studies, a small number of parameters were typically used to characterize the defects and the initial guesses were often selected extremely close to the actual values. In addition, a relatively large number of iterations were often required to obtain a convergent solution.

Through the modification of the numerical components, there are numerous opportunities to enhance the methods for identifying subsurface defects. Several of these numerical enhancements are incorporated into the solution procedure proposed in this thesis study, and will be discussed further in subsequent chapters. Before discussing the problem of subsurface cavity detection any further, it should be clarified that the example problems, analysis, and the comparison with previous research was conducted in a numerical sense and word enhancement is with reference to the previously described numerical procedures.

1.1.3 Crack Propagation

Fiber-reinforced composite materials are used extensively for a variety of high performance components. The heterogeneous and non-isotropic nature of these materials makes the prediction of their response more challenging than typical isotropic engineering materials.

However, the increased use of these materials is warranted due to their: high-strength, high-stiffness, low density, resistance to fatigue and corrosion, and their ability to be customized. The response of composite materials to damage caused by internal cracks is of importance because many primary load bearing structures use these materials.

Different materials and loading conditions can cause a crack to propagate in various manners. Shanyi et al. [16], Shan et al. [17], Hoff [18] and Dodd's et al. [19] have studied crack growth in ductile materials, which exhibit a period of stable crack growth prior to the onset of unstable or fast fracture. Miyazaki et al. [20] have extended these studies to include inhomogeneous materials by considering crack extension which was perpendicular to a bimaterial interface. Nishioka et al. [21] have examined the dynamic aspects of crack propagation by considering unstable, constant-velocity crack growth. A variety of finite element techniques can be used to simulate the growth of these cracks. A number of these techniques are discussed by Liebowitz and Moyer [22]. The most commonly used modelling procedure is the nodal release method [23], which releases, or "unpins", a displacement constraint at the crack tip when a predefined fracture criterion has been satisfied. The crack tip is then advanced to the adjacent node in the direction of crack propagation. The displacement constraint, removed from the previous crack tip node, is replaced by an equivalent force which is incrementally reduced to zero during subsequent iterations of the analysis. This procedure can be repeated for the entire duration of crack growth. Although the nodal release method and the other techniques presented by Liebowitz and Moyer are capable of determining the length of stable fracture, the critical crack length, and crack arrest length, they have an inherent deficiency in that the direction of crack extension must be known *a priori*. In the

previously mentioned references, the direction of crack growth was known because the numerical models were constructed such that the crack tip experienced a pure mode I loading, which is known to produce self-similar crack extension. For mixed mode loading conditions, however, the crack does not propagate in the same direction as the original crack , so the previously described techniques for modeling crack extension become difficult to apply.

A crack can be subjected to mixed mode loading conditions if the applied load is not perpendicular to the direction of the crack, or if the materials in a heterogeneous domain differ in elastic properties. Although, Mahanty and Maiti [24] studied the effects of mixed mode loading conditions on stable crack growth using a nodal release type method, but, the initial direction of crack growth was determined prior to the finite element analysis and the stable growth was restricted to taking place in a straight line along this direction. Many other researchers [25-37] have recognized the importance of mixed mode fracture mechanics, which has generated a considerable amount of research in this area. From this research, two main approaches for determining the direction of crack growth under mixed mode loading conditions have arisen; one approach utilizes the energy of the system while the other considers stress parameters.

The maximum tangential stress theory, developed by Erdogan and Sih [25], is based on the hypothesis that crack growth in a brittle material will start at the tip of the crack in the radial direction which corresponds to the plane perpendicular to the direction of greatest tangential stress. Further, they state that if the Griffith theory [38] is accepted as a valid fracture criterion, then a crack will grow in a direction along which the elastic energy released per unit of crack extension is a maximum and the crack will start to grow when a critical value

of this energy is reached. This theory is commonly referred to as the maximum energy release rate criterion.

The other widely accepted mixed mode fracture theory, as presented by Sih [34], is the minimum strain energy density. This theory assumes that crack extension occurs in the direction of minimum strain energy density. Sih and Barthelemy [30] recognized that for structures with complex geometries and loading conditions, or for applications where the loading direction could vary during service, the direction of crack growth is not constant. Sih and Barthelemy utilized the minimum strain energy density criterion to study the problem of fatigue, or sub-critical crack extension, subject to mixed mode cyclic loading. Tanaka [31], as well as Chen and Keer [32], have proposed sub-critical crack growth models for mixed mode cyclic loading conditions based on effective stress intensity values. Swedlow [33] provides a brief literature review of mixed mode fracture mechanics for homogeneous materials.

The increased use of composite materials has prompted considerable examination of interfacial cracks between dissimilar materials [39-51]. An analytical expression for the stress distribution surrounding an interfacial crack has been developed [39] and is based on bimaterial constants which account for the mismatch of elastic or thermal properties of the two materials. With this solution for the local stress field, the maximum tangential stress theory can be used to predict the direction and conditions required for crack growth [40]. The stress field derivation is based on a crack coincident with the material interface. A similar relationship has been developed for a kinked crack running parallel to the interface [41]. Unfortunately, an analytical relationship for a crack with an arbitrary orientation with respect to an arbitrarily shaped interface is not available in the literature.

An alternate approach to examining the behavior of interfacial cracks is to consider the energy release rate associated with a kinked crack [42-44]. For this analysis the crack is extended in a kinked manner by a small amount at various angles with respect to the original crack direction. The energy release rate can be numerically evaluated at each angle and then the angle of crack extension can be predicted using the maximum energy release rate criterion.

The determination of the crack growth direction by means of maximizing the strain energy release rate is, in fact, an inverse problem. The treatment of crack growth as an inverse problem does not appear in the literature. Consequently, an inverse solution procedure is developed here to determine the direction of crack growth in a heterogeneous domain.

1.2 Definition of Problems

1.2.1 Subsurface Cavity/Inclusion Detection

The inverse problem of subsurface cavity detection may be considered a nondestructive inspection technique that is typically used for determining system parameters, such as the interior geometry and material properties, when the inputs (loading and structural constraints) are specified and a portion of the output (displacement) is known.

Figure 1.1 displays a general schematic of this inverse problem. A two-dimensional, isotropic, homogeneous and linear elastic domain Γ, having a boundary $\partial\Gamma$, is comprised of two subdomains, the matrix Γ_1 and the cavity or inclusion Γ_2. The two subdomains share a common interface $\partial\Gamma_I$.

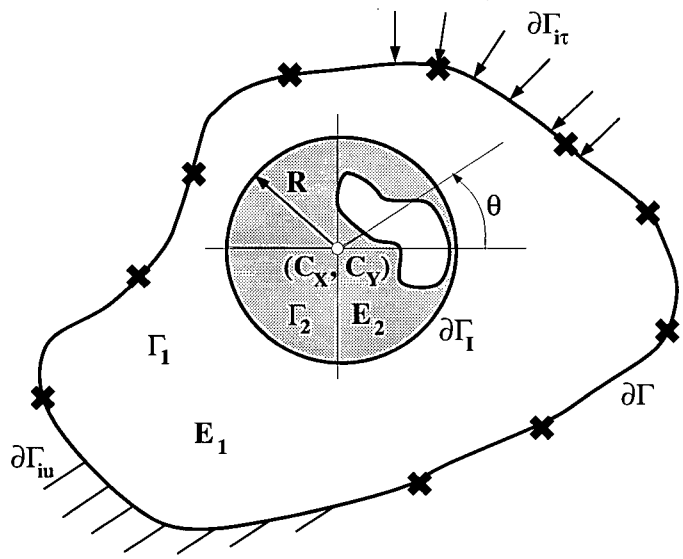

Figure 1.1: Definition of the subsurface parameter identification problem (sensor locations, $\check{s}^k$ (k=1,N), are indicated by ✖). The objective of the inverse analysis is to determine C_X, C_Y, R, θ and E_2.

The following equations, in indicial form, govern the behavior in each domain of this elastic problem.

From equilibrium

$$\sigma_{ij,j} + f_i^b = 0 \tag{1.1}$$

For small strains

$$\varepsilon_{ij} = \frac{1}{2}(u_{i,j} + u_{j,i}) \tag{1.2}$$

from Hooke's law

$$\sigma_{ij} = \lambda\varepsilon_{kk}\delta_{ij} + 2\mu\varepsilon_{ij} \tag{1.3}$$

Where Lame constants are

$$\lambda = \frac{\nu E}{(1+\nu)(1-2\nu)}, \quad \mu = \frac{E}{2(1+\nu)} \tag{1.4}$$

With prescribed displacements $\hat{u}_i$ and tractions on $\partial\Gamma$

$$\begin{aligned} u_i(s) &= \hat{u}_i(s) \quad \text{on} \quad s \in \partial\Gamma_{iu} \\ \tau_i(s) &= \hat{\tau}_i(s) \quad \text{on} \quad s \in \partial\Gamma_{i\tau} \end{aligned} \tag{1.5}$$

where i and j=1,2 for a two dimensional problem.

It is assumed that there exists a set of sensor points $\check{s}^k$ (k=1 to N) on the boundary of the structure where the measured displacement response u_i^k can be obtained. In addition, the experimental error associated with these measured displacements is assumed to be negligible, therefore, u_i^k are identical to the true displacements $\hat{u}_i^k$ at the sensor locations.

$$u_i\left(\check{s}^k\right) \approx \hat{u}_i^k \qquad \check{s}^k \in \partial\Gamma \qquad i = 1,2 \quad k = 1,N \tag{1.6}$$

Practically, the approximate value of these exterior displacements would be obtained using experimental methods such as strain gauges, holographic interferometry, laser speckle interferometry, etc. The objective of the inverse analysis is to determine the system parameters associated with the inclusion; e.g. the centroid (C_X, C_Y), radius , R, angle of rotation, θ, and Young's modulus E_2. Collectively, these unknowns are often referred to as the design variable vector or parameter vector. The Young's modulus of Γ_1 and the Poisson's ratio of Γ_1 and Γ_2 are assumed to be known.

1.2.2 Crack Propagation

Figure 1.2 is a general schematic of the inverse problem of determining the direction a crack will propagate in a heterogeneous domain. A crack tip increment of length Δa and unknown orientation θ, is contained within the boundary $\partial\Gamma$ of a two-dimensional domain which is subject to boundary forces on $\partial\Gamma_{i\tau}$ and prescribed displacements on $\partial\Gamma_{iu}$. Multiple

subdomains Γ_i of differing material properties may be contained within $\partial\Gamma$. Each domain is assumed to be isotropic, linearly elastic, and under plane strain conditions. The objective of the analysis is to determine in what direction θ the crack will propagate given that it grows by a length Δa.

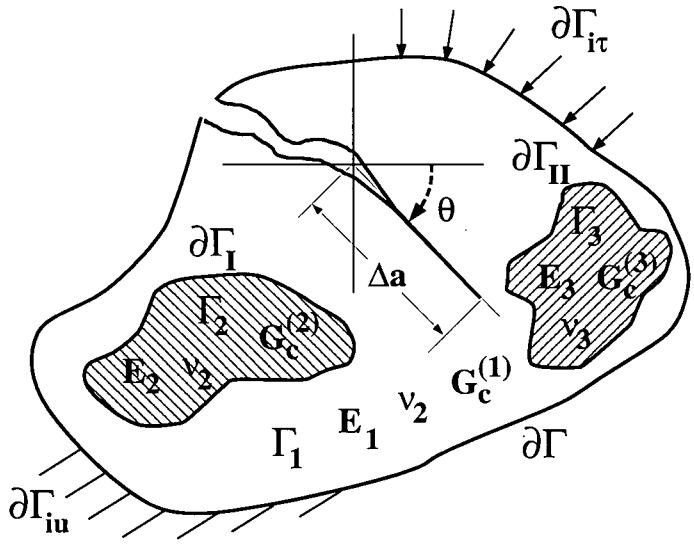

Figure 1.2: Definition of the crack propagation problem. The objective of the inverse analysis is to determine θ.

The angle of crack extension associated with the maximum energy release rate is independent of the magnitude of the applied load. Therefore, no consideration is given to whether the conditions for crack growth are satisfied (i.e. whether the applied load is sufficient to cause crack extension). The crack is subjected to a gradually applied monotonic load† or a sub-critical cyclic loading‡ and the objective is to determine the path it will follow. Equations (1.1) - (1.5) govern the behavior of this elastic problem in each domain. The notation E_i, ν_i and $G_c^{(i)}$ in Figure 1.2 refer to the Young's modulus, Poisson's ratio and the critical energy release rate for each domain Γ_i.

† Dynamic effects are assumed to be negligible ($da/dt \approx 0$).

‡ It is also assumed that the direction of crack extension for monotonic and cyclic loading is approximately the same [30].

1.3 Objectives

By examining previous research related to the numerical identification of subsurface flaws, several opportunities for enhancement can be recognized. Consequently, an enhanced solution procedure for the numerical detection of internal defects is proposed here. The modifications are accomplished by utilizing finite element substructuring techniques to reduce computation effort and by incorporating a sophisticated Quasi-Newton type algorithm to update the system parameters. A procedure that integrates these numerical components is presented in Chapter 2 and the models and results of the numerical study are given in Chapter 3. These results verify the accuracy and efficiency of the proposed procedure. Again, it should be realized that the enhancements proposed in this thesis are with respect to the numerical procedures presented in the literature. These modifications are intended to aid in the nondestructive evaluation of actual engineering structures in the future.

As previously mentioned, the treatment of crack growth as an inverse problem does not appear in the literature. As a result, a mathematical formulation of this inverse problem, which utilizes the finite element method and optimization techniques for its solution, is presented here. More specifically, a procedure concerned with maximizing the energy release rate of the system is proposed for determining the direction in which a crack will propagate in a heterogeneous domain. The procedure is verified through a numerical study which examines four fracture cases of increasing complexity and yields results which are consistent with both theoretical and experimental findings.

Chapter 2

Numerical Developments

2.1 The Finite Element Method

2.1.1 Introduction

It is well known that the finite element method (FEM) can be used to solve complex problems in solid mechanics if the information for solving the direct problem is given. Other numerical techniques such as the boundary element method and the finite difference method can also be used. The finite element method has been chosen because it has enhanced features such as automatic meshing and the ability to accommodate inhomogeneous materials and nonlinear material behavior. Although the numerical examples considered here are for homogeneous domains and linear elastic behavior, extending the solution to more complex problems is possible. In addition, commercially available codes can be readily integrated into the solution procedure and are quite reliable for solving the required static analysis.

To solve inverse parameter identification problems, the FEM is required to solve a series of direct problems. The relationship between the FEM and inverse identification problems can be seen by examining the standard finite element equation for a static analysis:

$$[K]\{u\}=\{f\} \tag{2.1}$$

where [K] is the assembled (reduced) global stiffness matrix, {u} is the nodal displacement vector, and {f} is the nodal force vector.

If the material properties and geometry are known, the stiffness matrix [K] can be obtained and a direct problem solved to determine the system response. Therefore, for the first iteration of the inverse analysis, the design variables must be assigned appropriate (guess) values. For subsequent iterations, optimization techniques are used to update the design variables which then allows additional forward problems to be solved.

The commercially available finite element code, ANSYS, is used to perform the finite element analyses required for the numerical study conducted in Chapter 3.

2.1.2 Crack Tip Elements (Singular Elements)

In many practical situations, internal cracks may be present in a structure. Identifying such a defect, or determining its growth behavior requires that the cracked be modelled correctly.

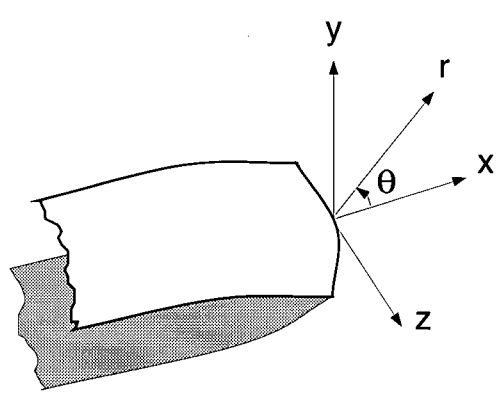

Figure 2.1: Coordinate system used for a three-dimensional crack front.

For the general three-dimensional crack front shown in Figure 2.1, the stress field surrounding

this region has the form [22]

$$\sigma_{ij} = \frac{K_I}{\sqrt{2\pi r}} g_{ij}^{I}(\theta) + \frac{K_{II}}{\sqrt{2\pi r}} g_{ij}^{II}(\theta) + \frac{K_{III}}{\sqrt{2\pi r}} g_{ij}^{III}(\theta) \tag{2.2}$$

where K_I, K_{II}, K_{III} are the stress intensity factors associated with the the three modes of fracture, and $g_{ij}(\theta)$ are angle-dependent expressions related to the geometry of the structure. From this equation, the stress field becomes infinite as r approaches zero ($1/\sqrt{r}$ singularity) and so to obtain accurate values of the stress field or stress intensity factors (K_I, K_{II}, K_{III}) the $1/\sqrt{r}$ singularity must be taken into consideration.

Elements capable of representing the $1/\sqrt{r}$ stress/strain singularity have been incorporated into the FEM. It was found that by placing the midside nodes of a standard 8-noded isoparametric element at the one-quarter point position, the element strain field exhibits the square root singularity [52]. This technique of repositioning nodes within an element to produce a singularity in the approximating function is conveniently described by considering a one-dimensional quadratic isoparametric case [53]. Figure 2.2 shows a 3-noded parabolic element with the three nodal locations specified in the physical x-space and the standard element ζ-space. The element shape functions N_i are also included in this figure.

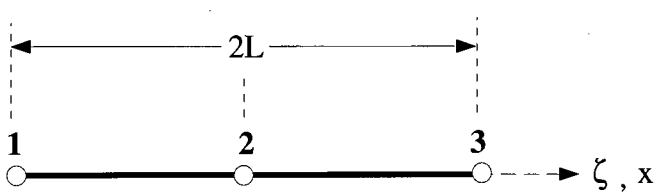

x-space:	x_i	$x_{i+1}=x_i+qL$	$x_{i+2}=x_i+2L$	$N_i = \frac{1}{2}\zeta_i\zeta(1+\zeta_i\zeta)$; i=1,3
ζ-space:	$\zeta_1=-1$	$\zeta_2=0$	$\zeta_3=1$	$N_i = (1-\zeta^2)$; i=2

Figure 2.2: 3-noded parabolic element including x-space, ζ-space and shape functions N_i.

The expression relating the x-space and shape functions is

$$\mathbf{x}(\zeta) = \sum_{i=1}^{3} N_i(\zeta) x_i \tag{2.2}$$

which can be expressed as

$$x(\zeta) = x_i \frac{\zeta(\zeta - 1)}{2} + x_{i+1}\left(1 - \zeta^2\right) + x_{i+2} \frac{\zeta(\zeta + 1)}{2} \tag{2.3}$$

Similarly, the displacement of the element u may expressed in terms of the nodal displacements $\hat{u}_i$ by

$$u(\zeta) = \sum_{i=1}^{3} N_i(\zeta) \hat{u}_i \tag{2.4}$$

which gives

$$u(\zeta) = (\hat{u})_{i+1} + \frac{\zeta}{2}\{(\hat{u})_{i+2} - \hat{u}_i\} + \frac{\zeta^2}{2}\{(\hat{u})_{i+2} - 2(\hat{u})_{i+1} + \hat{u}_i\} \tag{2.5}$$

If q is assigned the value of one-half, node 2 is placed at the quarter point position between x_i and x_{i+2}, then from equation (2.3)

$$\zeta = \left\{\frac{2(x + x_i)}{L}\right\}^{\frac{1}{2}} - 1 \tag{2.6}$$

Substituting equation (2.6) into equation (2.5) yields

$$u(x) = a + b\sqrt{(x - x_i)} + c(x - x_i) \tag{2.7}$$

where a, b and c are functions of u_i, u_{i+1} and u_{i+2}. Differentiating equation (2.7) results in the required $1/\sqrt{r}$ singularity for the strain. The nodal displacement method used here is a convenient way of simulating the singular stress/strain field in the vicinity of the crack tip and can be easily incorporated into most standard FE codes.

To use these elements correctly, x_i should be located at the tip of the crack. To represent this singularity in two or three dimensions, the singular elements should surround the entire crack tip/front. Figure 2.3 shows two typical singular elements and illustrates how they

should be positioned with respect to the crack tip/front. With the proper use of these singular elements, the stress/strain fields in the vicinity of the crack tip may be represented more effectively than with the use of regular elements..

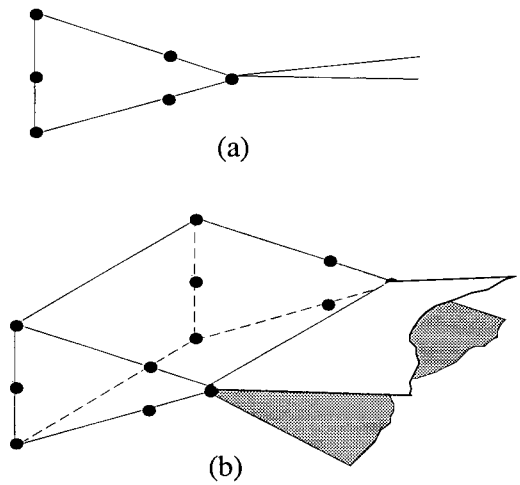

Figure 2.3: (a) 2-D singular element (6 or collapsed 8-noded elements) and (b) 3-D singular element (15 or collapsed 20-noded elements). These elements should encircle the entire crack tip/front.

2.1.3 Substructuring Techniques

Substructuring is a procedure that condenses several finite elements into one equivalent or super element. The condensation is accomplished by identifying two separate degree of freedom groups , the master (retained) degrees of freedom (DOF) and the slave (removed) DOF. For a static analysis, equation 2.1 takes the form [54]:

$$\begin{bmatrix} [K_{mm}] & [K_{ms}] \\ [K_{sm}] & [K_{ss}] \end{bmatrix} \begin{Bmatrix} \{u_m\} \\ \{u_s\} \end{Bmatrix} = \begin{Bmatrix} \{F_m\} \\ \{F_s\} \end{Bmatrix} \tag{2.8}$$

where m and s represent master and slave, respectively. Equation 2.8 can be rewritten as:

$$\left[\hat{K}\right]\{u_m\} = \left\{\hat{F}\right\} \tag{2.9}$$

where

$$\left[\hat{K}\right] = [K_{mm}] - [K_{ms}][K_{ss}]^{-1}[K_{sm}] \tag{2.10}$$

and

$$\left\{\hat{F}\right\} = \{F_m\} - [K_{ms}][K_{ss}]^{-1}\{F_s\} \tag{2.11}$$

The new condensed stiffness matrix represents the stiffness of what is referred to as a superelement. This element may be used the same way as any other element type. Substructuring is accomplished by three separate analyses or passes: the generation pass, the use pass and the expansion pass.

The generation pass is used to combine "regular" elements into the single superelement. The use pass simply incorporates the superelement into the complete model and obtains a solution; whereas the expansion pass is required if the results within the superelement are desired.

The specific application of subsurface cavity detection is ideally suited for incorporating substructuring techniques since only the stiffness characteristics of the defect are of importance and not its interior response. As a result, substantial computational savings can be realized because the expansion pass used to calculate the behavior within the superelement is not required. Further computational savings are realized when automeshing the model.

2.2 Optimization Techniques

2.2.1 Introduction

Optimization is the search for the minimum or maximum of a function. This function

is commonly referred to as the cost or objective function and is dependent on the design variable vector, $\mathbf{x}=(x_1,x_2, \ldots, x_n)$, which contains the unknown system parameters. The objective of the optimization process is to determine the values of these design variables which minimize the cost function. In addition to minimizing the objective function, the design may have to meet or satisfy certain criteria or specifications. These restrictions on the minimization process may be represented mathematically by what are known as constraint equations. For certain classes of problems, linear programming for example, there are techniques which calculate a unique global minimum of the cost function in a relatively short period of time. However, with the exception of a limited number of applications, most practical engineering problems require constrained nonlinear programming (NLP). The majority of constrained nonlinear programming algorithms expect the problem to be in the following standard optimization form [55]:

$$\begin{gathered}\text{Minimize}\\ f(\mathbf{x})\\ \text{subject to}\\ h_j(\mathbf{x}) = 0; \qquad j = 1 \text{ to } p\\ g_j(\mathbf{x}) \geq 0; \qquad j = 1 \text{ to } m\\ x_i^{(L)} \leq x_i \leq x_i^{(U)}; \qquad i = 1 \text{ to } n\end{gathered} \tag{2.12}$$

where $f(\mathbf{x})$ is the objective function or quantity to be minimized and p and m are the number of equality and inequality constraints, respectively. The vector of independent or design variables is $\mathbf{x}$ and the lower and upper bounds of each of the design variables are $\mathbf{x}^{(L)}$ and $\mathbf{x}^{(U)}$, respectively. At the optimal design point the vector $\mathbf{x}$ must satisfy all the equality and inequality constraints.

The optimization program used in this work is a FORTRAN subroutine called NLPQL [56-61], which is based on the sequential quadratic programming algorithm of Wilson, Han and Powell.

2.2.2 Sequential Quadratic Programming

In nonlinear optimization, some or all of the functions may be highly nonlinear. In addition, for many engineering applications the objective function is implicitly defined in terms of the design variables. This is the case when the cost function is obtained from the results of a finite element analysis. For these reasons, numerical methods are required for solving problems of this type. Of the many numerical methods that have been developed, the Quasi-Newton methods are generally accepted as being among those most effective for handling constrained optimization problems [55]. In the literature, these methods are commonly referred to as Quasi-Newton methods, constrained variable metric methods, sequential quadratic programming (SQP), or recursive quadratic programming methods. The Quasi-Newton methods used to solve unconstrained and constrained nonlinear programming problems are iterative in nature and are based on the following steps:

- Assign an initial starting or guess value for the design variable vector, $\mathbf{x}^{(0)}$.
- Determine a search direction $\mathbf{d}^{(k)}$ which tends to reduce the cost function.
- Compute a step size α_k along $\mathbf{d}^{(k)}$ which satisfies a descent criteria. Obtain the new design point from.

$$x^{(k+1)} = x^{(k)} + \alpha_k d^{(k)} \tag{2.13}$$

- Repeat these steps until a predefined optimality or convergence criteria is satisfied.

As previously mentioned, NLPQL is the SQP code used to update the system parameters for the inverse analysis. NLPQL is based on the Schittkoski's implementation [57] of the sequential quadratic programming algorithm of Wilson, Han and Powell. The remainder of this section is dedicated to discussing the details of this algorithm.

Calculating the descent direction $\mathbf{d}^{(k)}$ requires obtaining and solving a quadratic programming subproblem at the current design point. The derivation of the quadratic programming subproblem is as follows. Consider the design optimization problem:

$$\text{minimize:} \quad f(\mathbf{x}); \quad \text{subject to:} \quad h_j(\mathbf{x})=0; \; j=1 \text{ to } p \tag{2.14}$$

where all functions are assumed to be twice differentiable and the gradients of the constraints are linearly independent. It is common to derive the quadratic programming subproblem by considering only the equality constraints. The inequality constraints can easily be incorporated as the derivation progresses. The derivation is based on the Kuhn-Tucker necessary conditions of equation (2.14) and their iterative solution by Newton-Raphson's method for nonlinear equations. For the problem of minimizing (2.14), let $\mathbf{x}^*$ be a local minimum of the problem and a regular point (i.e. the gradient vectors of all the constraints at point $\mathbf{x}^*$ are linearly independent) and there are Lagrange multipliers v_j^*, j= 1 to p, that satisfy the following necessary conditions for optimality:

$$\begin{aligned} \frac{\partial f(\mathbf{x}^*)}{\partial x_i} + \sum_{j=1}^{p} v_j^* \frac{\partial h_j(\mathbf{x}^*)}{\partial x_i} &= 0 \;\; ; \quad i = 1 \text{ to } n \\ h_j(\mathbf{x}^*) &= 0 \;\; ; \quad j = 1 \text{ to } p \end{aligned} \tag{2.15}$$

It is convenient to write equation (2.15) in terms of a Lagrange function, defined by:

$$L(\mathbf{x}, v) = f(\mathbf{x}) - \sum_{j=1}^{p} v_j h_j(\mathbf{x}) \tag{2.16}$$

Thus, the necessary conditions for optimality at point $\mathbf{x}^*$ become:

$$\begin{aligned} \frac{\partial L(\mathbf{x}^*, \mathbf{v}^*)}{\partial x_i} &= \nabla L(\mathbf{x}^*, \mathbf{v}^*) = 0 \ ; \quad i = 1 \text{ to } n \\ \frac{\partial L(\mathbf{x}^*, \mathbf{v}^*)}{\partial v_j} &\equiv h_j(\mathbf{x}^*) = 0 \ ; \quad j = 1 \text{ to } p \end{aligned} \tag{2.17}$$

By using the iterative Newton-Raphson procedure to solve this system of nonlinear equations, defining the Hessian of the Lagrange function (or its approximation) $\nabla^2 L$ as $\mathbf{H}$, defining the search direction $\Delta\mathbf{x}^{(k)}$ as $\mathbf{d}^{(k)}$ and by representing the inequality constraints with a first order Taylor series expansion about the current design point, the following quadratic programming subproblem is obtained:

$$\begin{gathered} \text{Minimize} \\ \nabla f^T \mathbf{d} + \frac{1}{2} \mathbf{d}^T \mathbf{H} \mathbf{d} \\ \text{Subject to} \\ \nabla h_j\left(\mathbf{x}^{(k)}\right)^T \mathbf{d} + h_j\left(\mathbf{x}^{(k)}\right) = 0, \quad j = 1 \text{ to } p \\ \nabla g_j\left(\mathbf{x}^{(k)}\right)^T \mathbf{d} + g_j\left(\mathbf{x}^{(k)}\right) \geq 0, \quad j = 1 \text{ to } m \\ \mathbf{x}^{(l)} - \mathbf{x}^{(k)} \leq \mathbf{d} \leq \mathbf{x}^{(u)} - \mathbf{x}^{(k)} \end{gathered} \tag{2.18}$$

A more rigorous derivation of this subproblem is presented by Arora [55].

The Quasi-Newton methods are strengthened by using quadratic or second order information supplied by the Hessian of the Lagrange function. Typically, it would not be possible

to incorporate the Hessian into the quadratic subproblem. However, the Hessian of the Lagrange function may be approximated (updated) from first order information. NLPQL utilizes a modified version of the effective Hessian updating method known as the BFGS (Broyden-Fletcher-Goldfarb-Shanno) method [55]. The modification was introduced by Powell and implies that the updated Hessian $\mathbf{H}^{(k+1)}$ will remain positive definite when starting the algorithm with a positive definite matrix, e.g. $\mathbf{H}^{(0)}=\mathbf{I}$, which assures the theoretical convergence of the algorithm.

A brief description of the BFGS method incorporating Powell's modification is as follows:

$$H^{(k+1)} = H^{(k)} + D^{(k)} - E^{(k)} \tag{2.19}$$

where $\mathbf{D}^{(k)}$ and $\mathbf{E}^{(k)}$ are nxn matrices defined by:

$$\begin{aligned} D^{(k)} &= \frac{1}{\xi_3} w^{(k)} w^{(k)} \\ E^{(k)} &= \frac{1}{\xi_2} z^{(k)} z^{(k)} \end{aligned} \tag{2.20}$$

The modification vector $\mathbf{w}^{(k)}$ is introduced to avoid the possibility of an indefinite Hessian. The expression for $\mathbf{w}^{(k)}$ is:

$$w^{(k)} = \theta y^{(k)} + (1-\theta) z^{(k)} \tag{2.21}$$

which is a function of the gradient of the Lagrange function at two points:

$$y^{(k)} = \nabla L\left(x^{(k+1)}, u^{(k)}, v^{(k)}\right) - \nabla L\left(x^{(k)}, u^{(k)}, v^{(k)}\right) \tag{2.22}$$

In addition, several intermediate scalars and vectors are required:

$$
\begin{aligned}
\xi_1 &= s^{(k)} y^{(k)} \\
\xi_2 &= s^{(k)} z^{(k)} \\
\xi_3 &= s^{(k)} w^{(k)} \\
\theta &= \begin{cases} 1 & \xi_1 \geq 0.2\xi_2 \\ \dfrac{0.8\xi_2}{(\xi_2 - \xi_1)} & \text{Otherwise} \end{cases}
\end{aligned}
\tag{2.23}
$$

where the change in the design variables is

$$
\begin{aligned}
s^{(k)} &= \alpha_k d^{(k)} \\
z^{(k)} &= H^{(k)} s^{(k)}
\end{aligned}
\tag{2.24}
$$

Solving the quadratic subproblem for the search direction $\mathbf{d}^{(k)}$ is accomplished by a FORTRAN subroutine called QPSOL, which is a self-contained program based on an "active-set null-space method" developed by Gills et al. [62]. This subroutine is generally accepted as being highly sophisticated, efficient and robust [63]. Further comments and recommendations regarding the performance of QPSOL can be found in Thanedar et al. [63].

The calculation of the step length α_k is obtained by minimizing or satisfying a descent (merit) function. The descent function is created to incorporate the effects of constraint violations into the progression of the algorithm. No descent function is ideal and a number of different versions and modifications have been presented by researchers [55]. The descent function utilized by NLPQL incorporates Schittkoski's augmented Lagrangian descent

function which has the following form [56]:

$$\Phi = f(x) + P_1(v,h) + P_2(u,g) \tag{2.25}$$

where

$$\begin{aligned} P_1(v,h) &= \sum_{i=1}^{p}\left(v_i h_i + \frac{1}{2} r_i h_i^2\right) \\ P_2(u,g) &= \sum_{i=1}^{m}\begin{cases} u_i g_i + \frac{1}{2}\mu_i g_i^2 \ , & \text{if } \left(g_i + \frac{u_i}{\mu_i}\right) \geq 0 \\ \frac{1}{2}\frac{u_i^2}{\mu_i} \ , & \text{otherwise} \end{cases} \end{aligned} \tag{2.26}$$

v_i and u_i are the Lagrange multipliers for the equality and inequality constraints and r_i and μ_i represent the penalty parameters associated with these constraints and are defined by:

for the first iteration

$$r_i^{(0)} = \left|v_i^{(0)}\right| \quad ; \quad \mu_j^{(0)} = u_j^{(0)} \tag{2.27}$$

and for the following iterations

$$\begin{aligned} r_i^{(k)} &= \max\left\{\left|v_i^{(k)}\right|, \frac{1}{2}\left(r_i^{(k-1)} + \left|v_i^{(k)}\right|\right)\right\} \\ \mu_i^{k} &= \max\left\{u_i^{(k)}, \frac{1}{2}\mu_i^{(k-1)} + u_i^{(k)}\right\} \end{aligned} \tag{2.28}$$

To obtain the value of α_k, a line search procedure is conducted with respect to the descent function given in equation (2.25). NLPQL calculates α_k by minimizing the one-dimensional function

$$\phi(\alpha) = P(x + \alpha d, r) \tag{2.29}$$

using quadratic interpolation and an Armijo-type stopping criterion [60]. Details of this portion of the analysis are outlined by Schittkowski [56]. Once α_k is obtained, the new design point can be calculated using equation (2.13). The algorithm continues to calculate new

design points until the solution satisfies the convergence criterion. More precisely, given an arbitrarily chosen initial design point, the algorithm converges to a point which satisfies the necessary optimality conditions (Kuhn-Tucker point) defined by:

$$\begin{aligned} &\nabla L(\mathbf{x}^*) = 0 \\ &h_i(\mathbf{x}^*) = 0 \quad ; \; i = 1 \text{ to } p \\ &u_i^* \geq 0 \quad ; \; i = 1 \text{ to } m \\ &g_i(\mathbf{x}^*) \leq 0 \quad ; \; i = 1 \text{ to } m \\ &u_i^* g_i(\mathbf{x}^*) = 0 \; ; \; i = 1 \text{ to } m \end{aligned} \tag{2.30}$$

Upon convergence of the optimization algorithm, an occurrence which implies that a local minimum of the objective function has been obtained, NLPQL returns the objective function value, the design variable vector, and performance information, such as the total number of iterations, convergence condition, etc.

2.3 Energy Release Rate Criterion

As previously mentioned, the maximum energy release rate criterion predicts that crack extension will occur in the direction which produces the maximum strain energy release. This hypothesis is based on the Griffith criteria for fracture which states: "Crack growth can occur if the energy required to form an additional crack of size da can just be delivered by the system" [63]. Mathematically, this can be expressed as:

$$\frac{dU}{da} = \frac{dW}{da} \tag{2.31}$$

where U is the strain energy and W is the work expended (required) for fracture. dU/da is

referred to as the energy release rate or the crack extension force G, while dW/da is the energy required to form an additional free surface and is known as the crack resistance (force). The energy required to form an additional crack or free surface is material dependent and is referred to as the critical energy release rate G_c.

The maximum energy release rate criterion predicts that crack extension will occur in the direction θ for which G is a maximum G_{max}, since this is the direction in which G_c will first be exceeded. For numerical purposes, the energy release rate for a kinked crack can be calculated using the global energy method [42]. When this method is used, equation (2.31) has the following mathematical form:

$$G(\theta, a) = -\frac{U(\theta, a + \Delta a) - U(\theta_0, a)}{B\Delta a} \tag{2.32}$$

where B is the thickness of the plate, $U(\theta_0,a)$ is the total strain energy of the structure with the crack in its original configuration (no kinking), and $U(\theta,a+\Delta a)$ is the strain energy of the structure with the crack extended by length Δa in the direction θ (kinked crack configuration).

The objective here is to determine the angle which maximizes G at any increment of crack growth. For a given increment, $U(\theta_0,a)$, Δa, and B remain constant. From equation (2.32), the direction of maximum strain energy for the kinked crack $U(\theta,a+\Delta a)_{max}$ is equivalent to the direction which predicts G_{max}. Therefore, only the elastic energy of the structure needs to be considered to predict the direction of crack extension.

For a heterogeneous domain, the original crack may be positioned near one or more material interfaces. In this circumstance, the crack may have the potential to propagate into one of several domains Γ_i each with different elastic properties and surface energies $G_c^{(i)}$.

Under these conditions, the maximum strain energy theory should be modified and restated as: the crack will propagate into the domain Γ_i whose surface energy G_c is first exceeded by the corresponding G_{max} value, and the angle which predicts G_{max} also predicts the direction of crack propagation [43]. In addition to the above criterion, the strength of the interfacial bond between domains $G_c^{(int),j}$, must be considered. If the critical energy release rate of the interfacial bond is considerably less than that of the adjacent materials, then the crack may remain along the interface regardless of the loading condition. Therefore, for a heterogeneous structure, a solution procedure which incorporates the strain energy release rate criterion must consider the various domains and interfaces encountered by the kinked tip. More specifically, the direction of crack growth can be obtained by determining the kink angle associated with the maximum of the following two ratios:

$$\max\left\{\left(\frac{G_{max}}{G_c}\right)_i, \left(\frac{G^{(int)}}{G_c^{(int)}}\right)_j\right\} \tag{2.33}$$

where i is the number of domains and j the number of interfaces encountered by the crack tip.

Although equation (2.33) is convenient in a theoretical sense its numerical implementation becomes inefficient. To alleviate this problem, Δa is varied in length so that the kinked crack tip may only encounter one material interface. This modification does not affect the validity of equation (2.33), however, i and j are limited in range to a maximum of 2 and 1, respectively. The solution procedure presented in the following section discusses this issue in more detail.

2.4 Solution Procedure

2.4.1 Subsurface Cavity/Inclusion Detection

The method for solving this inverse parameter identification problem is based on obtaining (calculating) displacement values $\mathbf{u}^*$ at the sensor locations, using the finite element method, and comparing these with the measured displacements $\hat{\mathbf{u}}$. The objective is to achieve a zero value when comparing these two sets of displacements, in a least squares sense. Mathematically, this may be accomplished by minimizing the following objective function:

$$f(\mathbf{x}) = \{\mathbf{u}^*(\mathbf{x}) - \hat{\mathbf{u}}\}^T\{\mathbf{u}^*(\mathbf{x}) - \hat{\mathbf{u}}\} \tag{2.34}$$

where $\hat{\mathbf{u}}$ are the reference displacements u_i (i=1,2) at the k sensor locations $\check{s}^k$, i.e. $\hat{\mathbf{u}}=u_i(\check{s}^k)$. The numerically calculated displacements $\mathbf{u}^*$ at the sensor location are a function of the design variable vector $\mathbf{x}^T = \{C_X, C_Y, \theta, R, E\}$. The general procedure for solving this inverse problem is outlined as follows:

1) Initial (starting) values for the design variables (C_X, C_Y, θ, R, E) are arbitrarily assigned.

2) A forward FE problem is executed to obtain the displacements at the sensor locations.

3) The objective function is used to compare the calculated and measured displacements.

4) Optimization techniques are used to alter the parameter vector **x** such that the objective function value is reduced.

5) Steps 2 through 4 are repeated until **x** satisfies a required convergence criterion.

The numerical techniques described in the previous section, the finite element method (ANSYS), and sequential quadratic programming (NLPQL) can be combined into an automated

process to perform the above steps. This process is outlined in Figure 2.4.

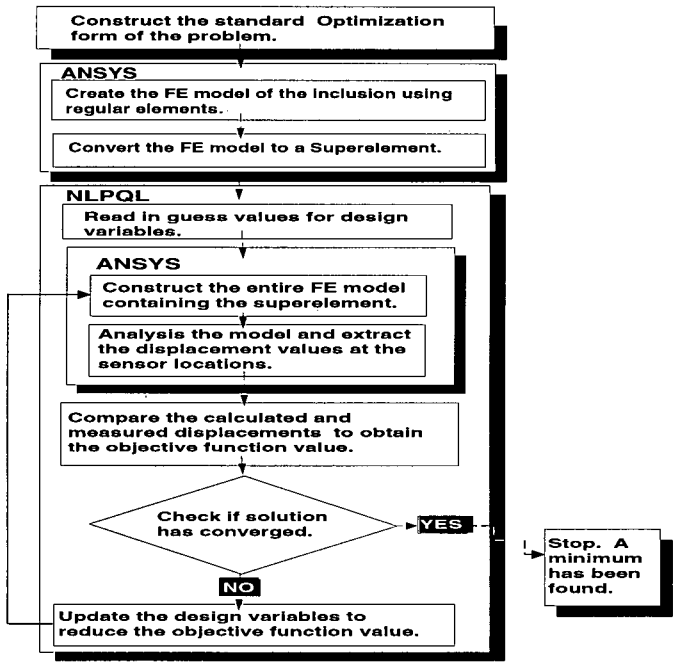

Figure 2.4: Automated process for solving the inverse parameter identification problem of subsurface cavity detection.

2.4.2 Crack Propagation

The following is a general description of the steps required to solve the inverse parameter identification problem of crack propagation through a heterogeneous domain. These steps and the required programming logic are described graphically by the flowchart in Figure 2.5. The lower case letters, **a** to **g**, in Figure 2.5 indicate the region of the flowchart corresponding to the description given in the following paragraphs, a. to g.:

a. To create a robust and efficient algorithm, the crack tip Δa is restricted in length so that a maximum of one interface may be encountered if Δa is rotated from its minimum to its maximum angular position such that the interface can be crossed only

once for a fixed value of θ. If the current length of Δa violates this requirement, the length of the crack tip is reduced by a small amount until a maximum of one interface lies within a circular arc of radius Δa centered at the tip of the previous increment of crack growth.

b. The initial guess value for the optimization algorithm can be one of two values depending on the regions encountered by the crack tip:

   i. If no interface is encountered, then the crack tip is in a region of material homogeneity and is assumed to travel in a straight line, therefore, the solution for the previous increment of growth θ^*_{m-1} is used as the starting value for the current increment $\theta^{(0)}_m$, i.e. $\theta^{(0)}_m=\theta^*_{m-1}$.

   ii. The only other possibility is that one material interface can be encountered. In this circumstance, if the two materials are assumed to be perfectly bonded then $\theta^{(0)}_m=\theta^*_{m-1}$, as described in i.; otherwise, $\theta^{(0)}_m$ is assigned the value of the angle which places the crack tip tangent to the interface, i.e. $\theta^{(0)}_m=\theta^{(int)}_m$.

c. The commercial finite element program ANSYS, is used to calculate the total strain energy of the structure at a given crack tip angle $\theta^{(k)}_m$ where m represents the current crack growth increment and k the current iteration of the optimization algorithm. For the initial (guess) value for θ, k equals 0. The SQP techniques described in the previous section (NLPQL) are then utilized to update the crack tip angle to increase, and ultimately maximize, the elastic energy release of the structure. The resulting angle θ^*_m represents the direction associated with the maximum energy

release rate for the current increment of crack growth.

d. If the crack tip is in a homogeneous region, then θ^*_m is the solution for the direction of crack growth and the crack is extended in that direction. The next increment of crack growth (m=m+1) is then considered. If not, the crack tip is in the vicinity of an interface between two materials. For discussion purposes, these materials will be referred to as Material 1 and Material 2. In addition, it is assumed that when the crack is kinked at the angle which represents the maximum energy release rate θ^*_m, the crack tip resides in Material 1. In this case, if the critical energy release rate of Material 1 ($G_c^{(1)}$) is less than that of Material 2 $G_c^{(2)}$) then crack extension will occur at the angle θ^*_m, unless the critical energy release rate of the interface $G_c^{(int)}$ is sufficiently low to cause $G^{(int)}/G_c^{(int)} > G_{max}/G_c^{(1)}$, in which case the crack will proceed tangentially along the interface. However, if $G_c^{(2)} < G_c^{(1)}$ then $G_{max}/G_c^{(1)}$ may not be greater than all $G(\theta)/G_c^{(2)}$ and the maximum value of $G(\theta)$ in Material 2 ($G_{max}^{(2)}$), must be determined.

e. If θ^*_m is less than $\theta^{(int)}_m$, then the crack tip resides in Material 2 for $\theta_m > \theta^{(int)}_m$. To find $G_{max}^{(2)}$ in this case, the lower bound for the standard optimization problem should be changed to $\theta^{(int)}_m$: i.e. $\theta^{(int)}_m < \theta_m < \theta^{(U)}_m$. Similarly, if θ_m is greater than $\theta^{(int)}_m$, the crack tip resides in Material 2 for $\theta_m < \theta^{(int)}_m$ and the upper bound should be altered ($\theta^{(L)}_m < \theta_m < \theta^{(int)}_m$) to solve for $G_{max}^{(2)}$.

f. Again, the finite element method and optimization techniques described previously are used to determine $G_{max}^{(2)}$.

g. At this stage, the three critical values:

$$\frac{G^{(int)}}{G_c^{(int)}}, \quad \frac{G_{max}}{G_c^{(1)}}, \quad \frac{G_{max}^{(2)}}{G_c^{(2)}}$$

have been obtained. The value of θ associated with the maximum value of these three ratios dictates the direction of crack extension for the current increment of growth. The next increment is then considered using the same procedure.

2.5 Discussion

To perform the numerical study presented in the following chapter, the numerical aspects and solution procedures discussed previously were combined using numerous FORTRAN subroutines, main control programs, and supporting data files. In addition, extensive ANSYS input files were required to perform the finite element analyses.

The finite element code was written to accommodate any geometric or material property changes dictated by NLPQL. The large number of function evaluations required for each inverse analysis excluded any user interaction with ANSYS. As a result, a substantial effort was involved in creating a "hands-off" finite element modelling procedure which could be executed in a background mode. To accomplish this, extensive use of ANSYS' parametric design language (APDL) [64] was required. For each finite element analysis, solid modelling techniques, Boolean operations, logical operators (conditional statements and loops), and post-processing commands were used for creating the model, obtaining a solution, error checking, and for retrieving results. In addition, a substantial amount of data file manipulation was required to supply information between ANSYS, NLPQL, and the supporting subroutines.

For the subsurface cavity detection problems, two finite element input files were created; one to construct the superelement (generation pass) and the other to create the entire model containing the superelement (use pass). Executing and combining these steps required a comprehensive understanding of ANSYS' substructuring capabilities and procedures. For a single model, these files contained over 200 programming statements.

The six crack propagation models examined in Chapter 3 required a more extensive use of programming logic and of APDL than the cavity detection problems. Each model required approximately 500 statements to create the model, complete the solution, and extract the total strain energy of the structure. The additional programming required for these models was a result of the complex geometry of the crack. In addition, the arbitrary location of the crack tip with respect to the material interface, as well as the concerns regarding automeshing and the modifications to the crack tip mesh, all introduced additional logic into the analysis.

The FORTRAN code written for both procedures required approximately 500 lines to initialize various parameters, combine NLPQL (≈2000 lines) and ANSYS, perform error checking, calculate the objective function values, calculate the value of the constraints, evaluate numerical derivatives, and create various data files for supplying information between programs. FORTRAN code was also written to modify certain sections of NLPQL.

The intent of our research group is conduct further research based on the work presented in this thesis. Therefore, it has been decide to treat this code as proprietary material and to limit its general distribution. For this reason, appendices containing the ANSYS input files and FORTRAN routines used in support of this research have not been included with this document.

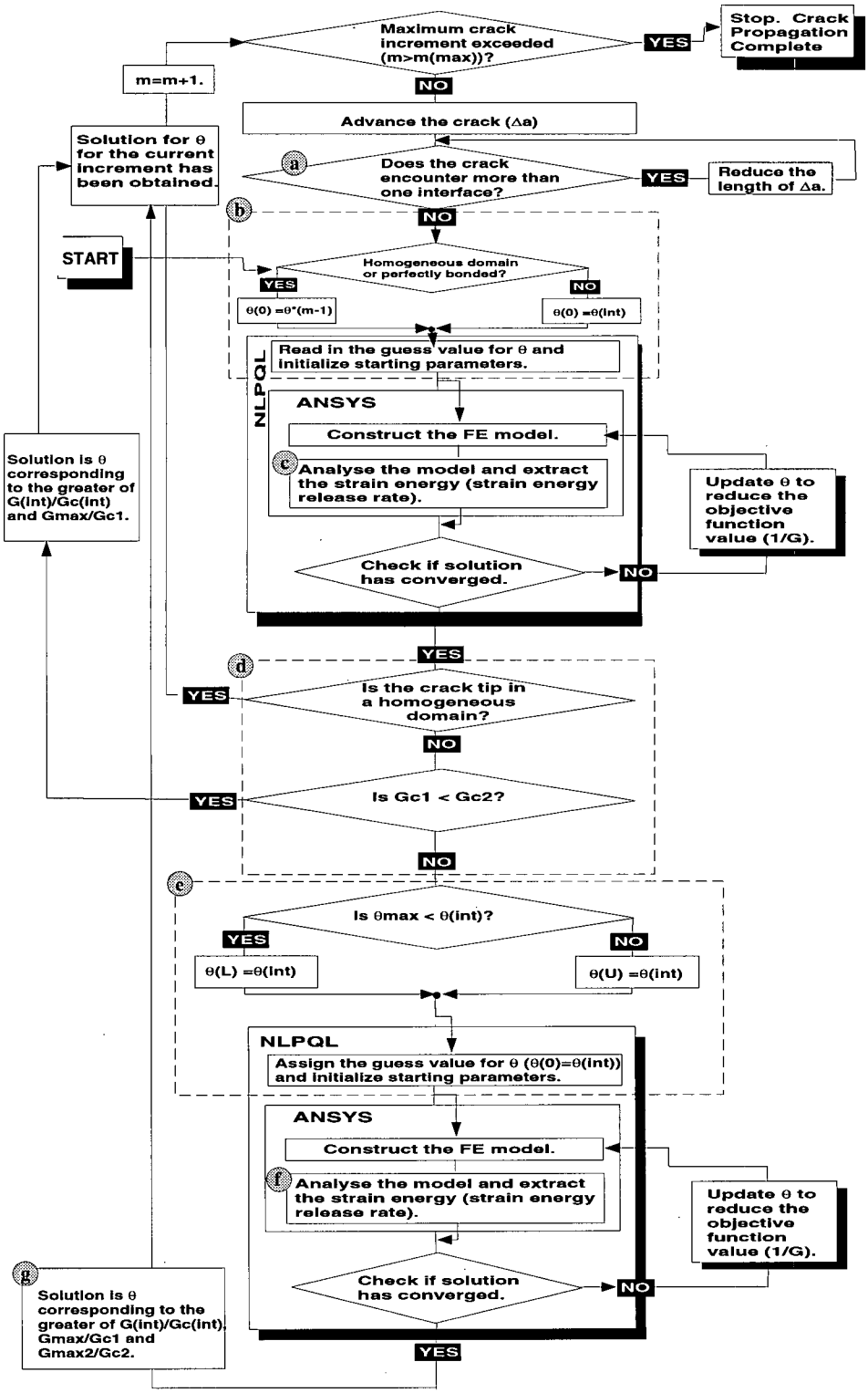

Figure 2.5: Automated process for solving the inverse problem of crack propagation through a heterogeneous domain.

Chapter 3

Numerical Study

3.1 Subsurface Cavity Detection

Two numerical examples are presented here to demonstrate the accuracy and effectiveness of the previously described algorithm. For generality, the first model, which consists of an inclusion with an arbitrarily shaped interior contained in an irregularly shaped matrix (plate), is considered. For a more practical application, the procedure is applied to the detection of a subsurface crack in a rectangular plate. Figures 3.1 and 3.6 show the geometry of the plate and inclusion, and the applied loading for both of these problems.

3.1.1 Generalized Model

Problem Description

From Figure 3.1 it can be seen that the generalized model consists of an inclusion, with a circular periphery and an arbitrarily chosen interior geometry, in an irregularly shaped plate. Traction and displacement boundary conditions are specified on the plate boundary.

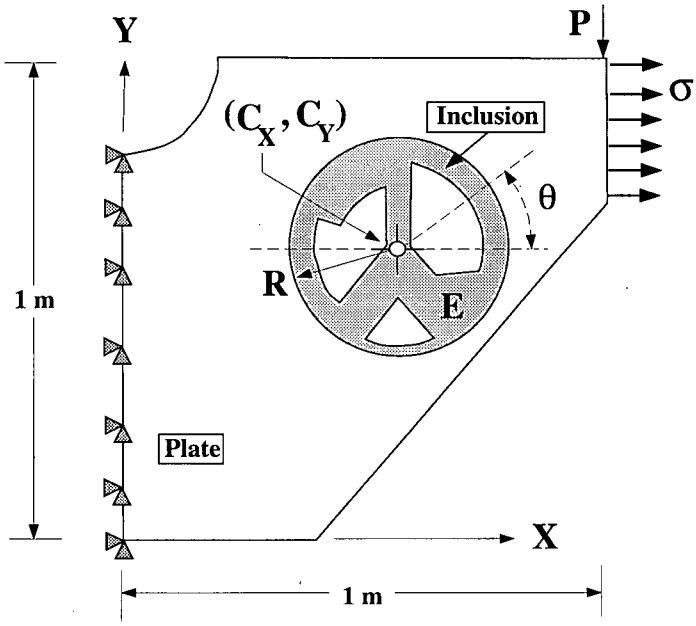

Figure 3.1: Generalized model (arbitrary inclusion and geometry). The objective is to determine the correct values of C_X, C_Y, θ, R and E.

As stated earlier, the complete inverse problem involves determining the Young's modulus of the inclusion E, its angle of rotation θ, the X and Y coordinates of the inclusion center C_X and C_Y, and the inclusion radius R, from the known applied traction and displacement boundary conditions and displacement measurements taken along the edges of the plate. To verify the solution procedure an initial study, which fixed the values of R, E, and θ, and solved for the true values of C_X and C_Y, was conducted. This approach allows the objective function to be plotted graphically as a function of C_X and C_Y, and enables the progress of the optimization algorithm to be monitored.

Finite Element Formulation

Figure 3.2 includes typical FE representations of the plate and inclusion and illustrates the substructuring process required to combine the superelement (inclusion) and regular elements (plate)..

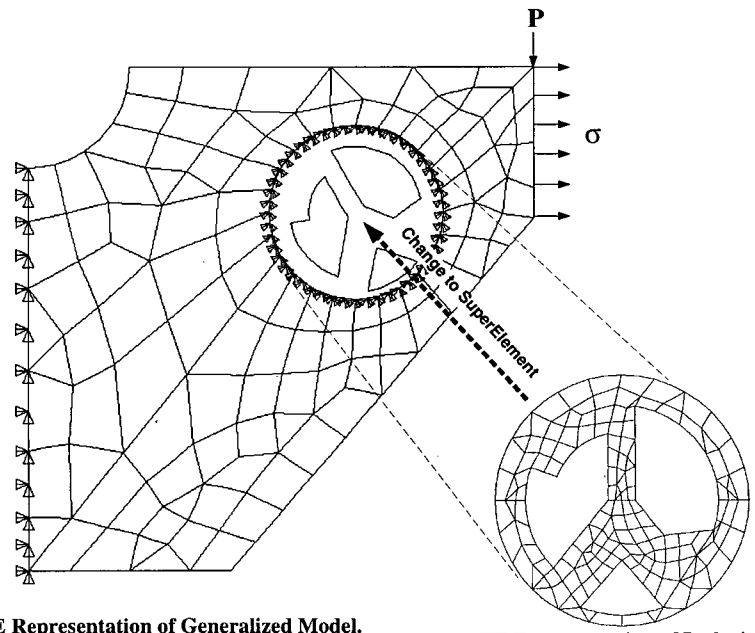

FE Representation of Generalized Model.

FE Representation of Inclusion using "Regular" Elements.

Figure 3.2: FE representation of generalized model and illustration of substructuring process.

The elements of the inclusion are condensed during the generation pass and the entire inclusion becomes a superelement that has only the degrees of freedom associated with the master nodes on the circumference of the element. The plate is constructed such that a circular hole, with the same radius and circumferential nodal locations as the superelement, is present. The superelement is then inserted into the circular hole and the coincident nodes and their corresponding DOF are coupled. The resulting model is equivalent to one that utilizes only regular elements. A static analysis is performed to determine the displacements at the

sensor locations. The sensors positions are assumed to coincide with the nodal locations on the free edges of the plate (81 nodes). The material behavior is assumed to be linear elastic and under plane strain conditions. The number of element divisions along the edges of the plate and around the circumference of the superelement remains constant for every iteration. The interior elements and nodes are created using ANSYS' automatic mesh generation capabilities.

The geometry and material properties of each model are dictated by NLPQL at every iteration of the inverse analysis. The function calls and derivative calculations required by NLPQL typically result in an excess of 100 direct finite element solutions, making a solution procedure which requires any user interaction with the FE modelling process infeasible. As a result, ANSYS input files were created that could accommodate any geometrical and material property changes dictated by the optimization algorithm. These input files utilize substructuring, solid modelling techniques, Boolean operations, data-file manipulation, error checking, and ANSYS' parametric design language (APDL) to perform each complete finite element analysis (pre-processing, solution and post-processing phases).

Formulation of Nonlinear Programming Problem

For the initial study, six constraints were used to keep the inclusion within the confines of the plate: two of which are functions of C_X and C_Y, one linear and the other nonlinear, and the remaining four specify their upper and lower bounds. From this information the standard optimization form of the problem becomes:

$$
\begin{aligned}
& f(C_X, C_Y) = \sum_{k=1}^{N} [(u_x^* - \widehat{u}_x)_k^2 + (u_y^* - \widehat{u}_y)_k^2] \\
& g_1: \quad C_X^2 + (1 - C_Y)^2 - 0.45^2 \geq 0; \qquad 0.25 \leq C_X \leq 0.75 \\
& g_2: \quad -\frac{7}{6} C_X + C_Y + 0.0825 \geq 0, \qquad 0.25 \leq C_Y \leq 0.75
\end{aligned}
\tag{3.1}
$$

For the complete study, which contains the entire set of design variables, sixteen constraints are required: six inequality constraints and ten which specify the upper and lower bounds on each design variable. The problem written in standard optimization form becomes:

$$
\begin{aligned}
& \text{Minimize:} \\
& f(C_X, C_Y) = \sum_{k=1}^{81} [(u_x - \widehat{u}_x)_k^2 + (u_y - \widehat{u}_y)_k^2] \\
& \text{Subject to:} \\
& g_1: \quad -(0.6X_4 + 0.25)^2 + (X_4(0 - X_1))^2 + (X_4(3 - X_2))^2 \geq 0 \qquad 0.25 \leq X_1 \leq 0.75 \\
& g_2: \quad X_4\left(X_2 + 1.4 - \frac{7}{6}X_1\right) - 0.385 \geq 0 \qquad 0.25 \leq X_2 \leq 0.75 \\
& g_3: \quad -X_4(0 - X_1) - 0.25 \geq 0 \qquad -359 \leq X_3 \leq 359 \\
& g_4: \quad X_4(3 - X_2) - 0.25 \geq 0 \qquad 0.17 \leq X_4 \leq 1.0 \\
& g_5: \quad -X_4(0 - X_2) - 0.25 \geq 0 \qquad 0.25 \leq X_5 \leq 2.0 \\
& g_6: \quad X_4(3 - X_1) - 0.25 \geq 0
\end{aligned}
\tag{3.2}
$$

When the problem is closed and bounded, the area enclosed by the constraints is known as the feasible region and the solution must be contained within this domain. For subsurface cavity detection, the feasible region is the area of the plate in which the center of the inclusion must remain. Figure 3.3 illustrates this by superimposing g_i (i=1 to 6) on the geometry of the generalized model.

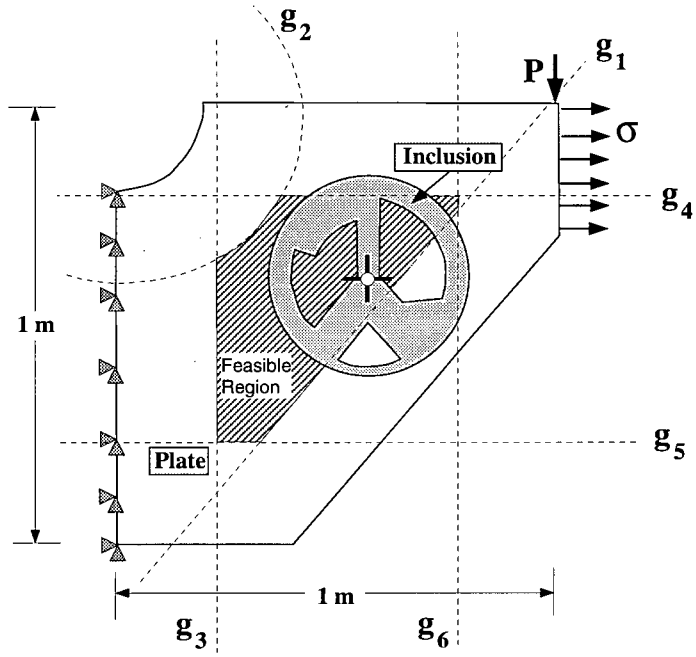

Figure 3.3: Physical representation of the constraints and feasible region. C_X and C_Y must remain within the feasible region.

Analytical expressions for the derivatives of the constraints, with respect to each design variable, are supplied to NLPQL through a user created subroutine. The derivatives of the objective function, with respect to each design variable, are calculated using a forward difference scheme.

Analysis and Results

In practice, the displacement data at the sensor locations would be obtained experimentally. For the purposes of this numerical study, the displacement values obtained from a direct finite element solution conducted using the correct actual design vector values were used as the reference data.

The parameter values corresponding to the correct solution are C_X=0.57 m, C_Y=0.61 m, E=1.0e7 N/m^2, R=0.23 m and θ=0°. The Young's modulus of the plate is 3.0e7 N/m^2 and the applied loads are 100 N and 150 N/m^2 for P and σ, respectively. It is important to realize that the magnitudes of E, R, θ, P, σ and the Young's modulus of the plate are arbitrary and the solution process is not dependent on their relative magnitudes. To solve the problem correctly, the only requirement on these variables is that they remain constant for the entire analysis.

For the initial study, the objective function was obtained by varying C_X and C_Y over the entire feasible region and evaluating equation (2.34) at each location (approximately 200 points in the feasible region). This data was used to create the objective function surface plot shown in Figure 3.4 (a). As expected, the objective function is a minimum and equals zero at C_X=0.57 m and C_Y=0.61 m. In addition to this global minimum, a local minimum exists in the vicinity of C_X=0.52 m and C_Y=0.75 m.

To test the algorithm, initial starting (guess) values of C_X=0.275 m and C_Y=0.3 m were assigned. The solution process is depicted in Figure 3.4. In Figure 3.4 (a), each iteration of the convergence process is superimposed on the objective function surface plot. After seven iterations, the objective function value is approximately zero and C_X and C_Y have converged to within 0.1% and 0.01% of their actual values, respectively. Figure 3.4 (b) depicts this convergence process in terms of the model geometry and a numerical summary of the analysis is given. From this single analysis, the algorithm performed exceptionally well.

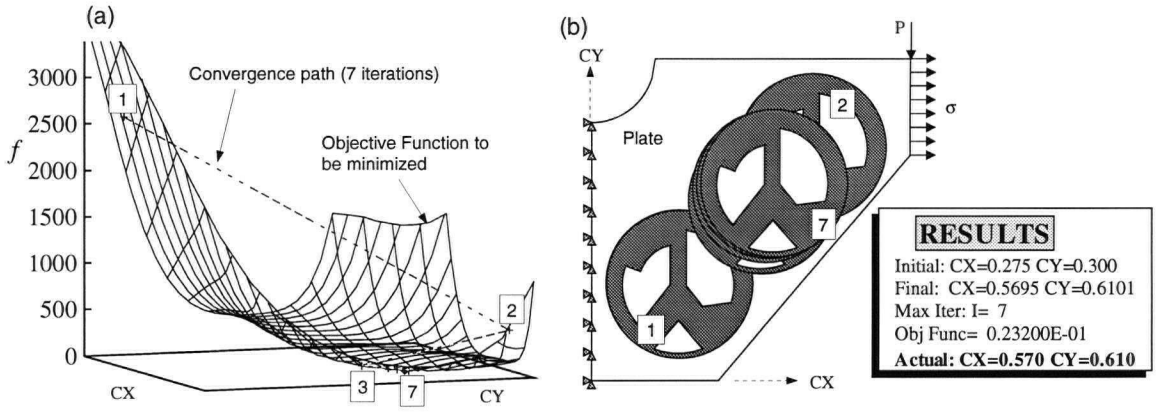

Figure 3.4: Convergence process for an arbitrarily shaped cavity: (a) Objective function surface plot with convergence path superimposed; (b) Plate and inclusion with iteration positions.

To further test the algorithm, the same problem was repeated seventeen times, each with a different (arbitrary) initial guess for C_X and C_Y. Thirteen of these solutions converged to the correct solution (global minimum), while the remaining four converged to the local minimum at C_X=0.52 m, C_Y=0.75 m. Since nonlinear optimization methods are unable to distinguish between a local and global minimum, all results should be accepted as successful solutions. It is recommended to solve nonlinear programming problems with a sequence of different starting points to aid in determining the global optimum.

For the extended study, the initial parameter vector $\mathbf{x}^T=\{C_X, C_Y\}$ was expanded to include 5 design variables; the radius of the inclusion R, its angle of rotation θ, and the Young's modulus E, of the inclusion, i.e. $\mathbf{x}^T=\{C_X, C_Y, \theta, R, E\}$. Therefore, in contrast to the initial study, it is not possible to visualize the objective function graphically. The convergence process can still be displayed in terms of the change in model geometry. The

convergence processes for the generalized model for two analyses, with different initial guesses for the design variables, are given in Figure 3.5. Also included in each figure are the guess values (Initial), final solution (Final), number of iterations (Max Iter), objective function value (Obj Func) at the solution and the correct (Actual) design variable values at the global minimum. A comparison of the actual values and final solution verifies the accuracy of the results.

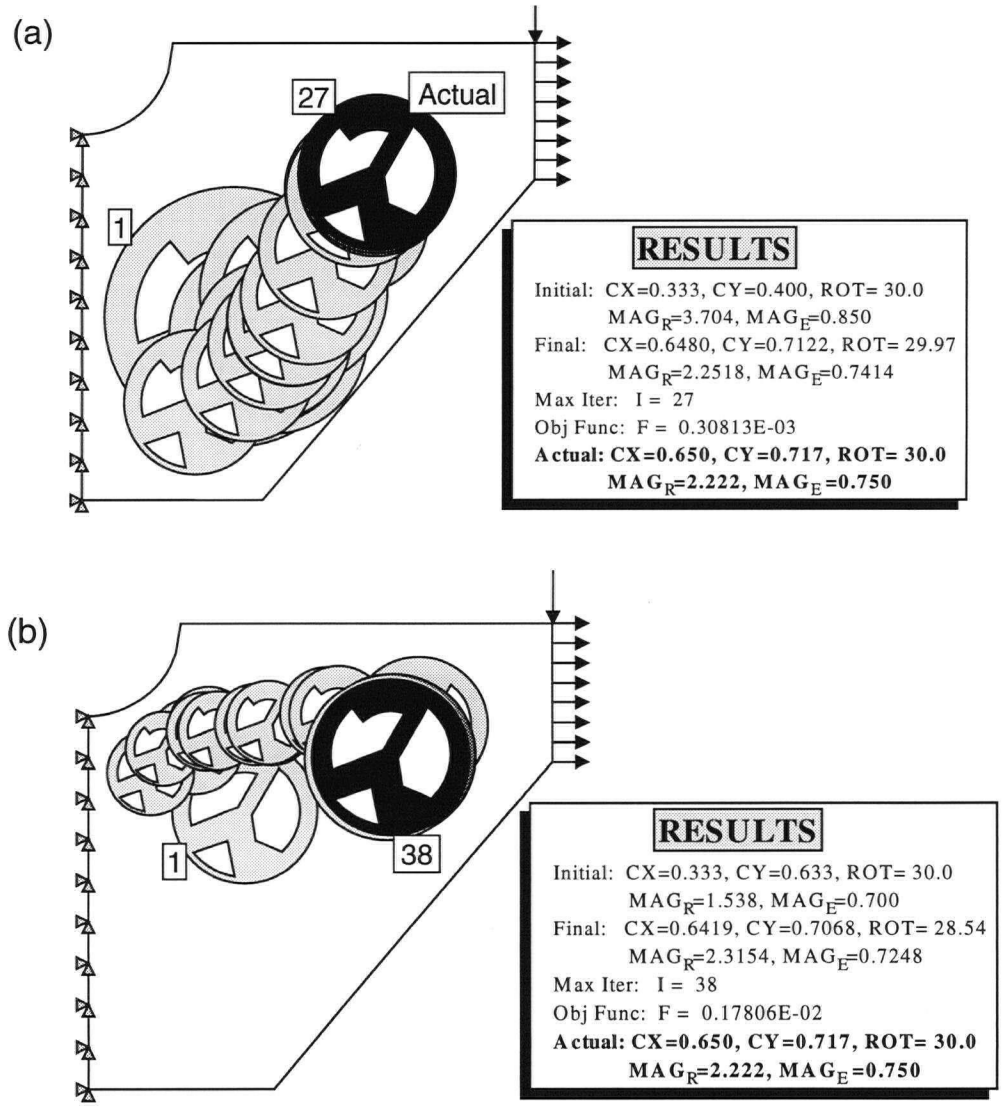

Figure 3.5: Convergence process for two different initial (guess) values.

3.1.2 Inclusion Containing a Through-Thickness Crack

Problem Description

The crack identification problem illustrated in Figure 3.6 is a specialized, more practical case of the generalized problem. The model is similar to the inclusion detection problem except that the circular defect, instead of containing an arbitrary geometry, surrounds a through thickness crack and is contained within a rectangular plate. Again, the traction and displacement boundary conditions are specified on the plate edges.

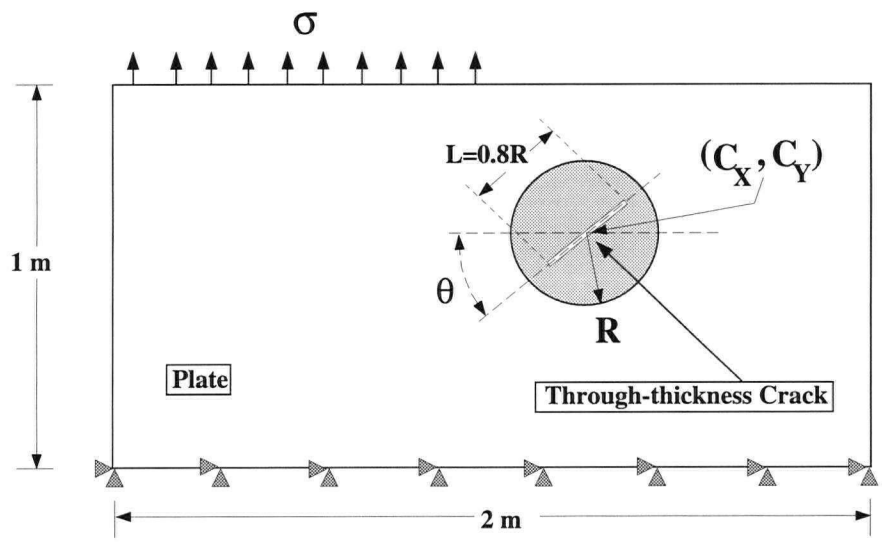

Figure 3.6: Inclusion containing a through-thickness crack. The objective is to determine the correct values of C_X, C_Y, θ, and R.

The complete inverse problem involves determining the radius of the inclusion R, its angle of rotation θ, and the X and Y coordinates of the inclusion center, C_X and C_Y, from the known applied traction and displacement boundary conditions, and from the measured displacements along the edges of the plate. The length of the crack is proportional to the radius of the inclusion (L=0.8R) and the Young's modulus of the inclusion is the same as the

plate; thus E is not a design variable as it was for the generalized model. Again, for the initial study, R and θ are fixed and the objective is to determine C_X and C_Y.

Finite Element Formulation

Figure 3.7 shows typical FE representations of the plate and the inclusion. Quarter-point elements are used to capture the singular strain field in the vicinity of the crack tip. Both crack tips, contained within the inclusion, are surrounded by nine singular elements. To represent a theoretically "ideal" crack, the crack faces are coincident. Again, the inclusion is converted into a superelement and combined with the regular elements of the plate. A static analysis is conducted to calculate the displacements at the sensor locations (approximately 120 nodal locations). The material behavior is assumed to be linear elastic and plane strain conditions apply.

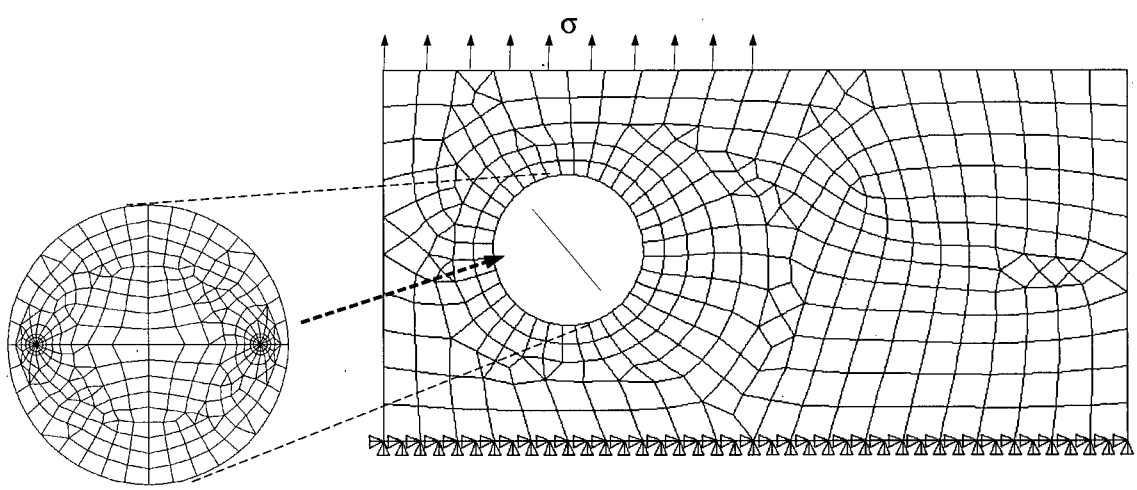

Figure 3.7: FE representation of crack detection model. Illustrates the substructuring process.

Formulation of Nonlinear Programming Problem

For the initial study, four constraints specifying the upper and lower bounds for C_X and

C_Y, are required to keep the inclusion within the confines of the plate. This problem has the following standard form:

$$f(C_X, C_Y) = \sum_{k=1}^{N} [(u_x^* - \widehat{u_x})_k^2 + (u_y^* - \widehat{u_y})_k^2] \tag{3.3}$$

$$0.22 \leq C_X \leq 1.78$$

$$0.22 \leq C_Y \leq 0.78$$

Since only the upper and lower bounds are specified, NLPQL does not calculate any constraint values or derivatives.

For the extended study, which considers the entire set of design variables, the rectangular feasible region was defined using four inequality constraints . Eight additional expressions were required to specify the upper and lower bounds on each design variable. The problem written in standard optimization form becomes:

Minimize:

$$f(C_X, C_Y) = \sum_{i=1}^{N} [(u_x^* - \widehat{u_x})_i^2 + (u_y^* - \widehat{u_y})_i^2] \tag{3.4}$$

Subject to:

g_1:	$-X_4(0 - X_1) - 0.05 \geq 0$	$0.25 \leq X_1 \leq 2.75$
g_2:	$X_4(3 - X_2) - 0.05 \geq 0$	$0.25 \leq X_2 \leq 2.75$
g_3:	$-X_4(0 - X_2) - 0.05 \geq 0$	$-359 \leq X_3 \leq 359$
g_4:	$X_4(3 - X_1) - 0.05 \geq 0$	$0.17 \leq X_4 \leq 1.0$

Once again, the derivatives of the objective function with respect to each design variable are calculated using a forward difference scheme.

Analysis and Results

The parameter values corresponding to the correct solution are C_X=0.35 m, C_Y=0.60 m, R=0.2 m and θ=0.0°. The Young's modulus of the plate and inclusion is 3.0e7 N/m^2 and the

applied load σ is 10000 N/m^2. R and θ remain constant during the analysis but C_X and C_Y are to be determined by the solution process.

The objective function surface plot shown in Figure 3.8 (a), was created using approximately 600 evenly spaced grid points in the feasible region. Each point corresponds to a different value for C_X and C_Y. The global minimum ($f(C_X,C_Y)=0$) is located at C_X=0.35 m and C_Y=0.60 m. In addition, a local minimum exists at C_X=1.75 m and C_Y=0.25 m. The analysis process used an initial guess of C_X=0.8 m and C_Y=0.55 m. Figure 3.8 (a) shows each iteration of the convergence process superimposed on the objective function surface plot. The solution required 11 iterations for C_X and C_Y to converge to within 0.03% and 0.08% of their respective actual values. Figure 3.8 (b) illustrates the convergence process with respect to the geometry of the model and summarizes the results numerically. The results for this single analysis are extremely accurate.

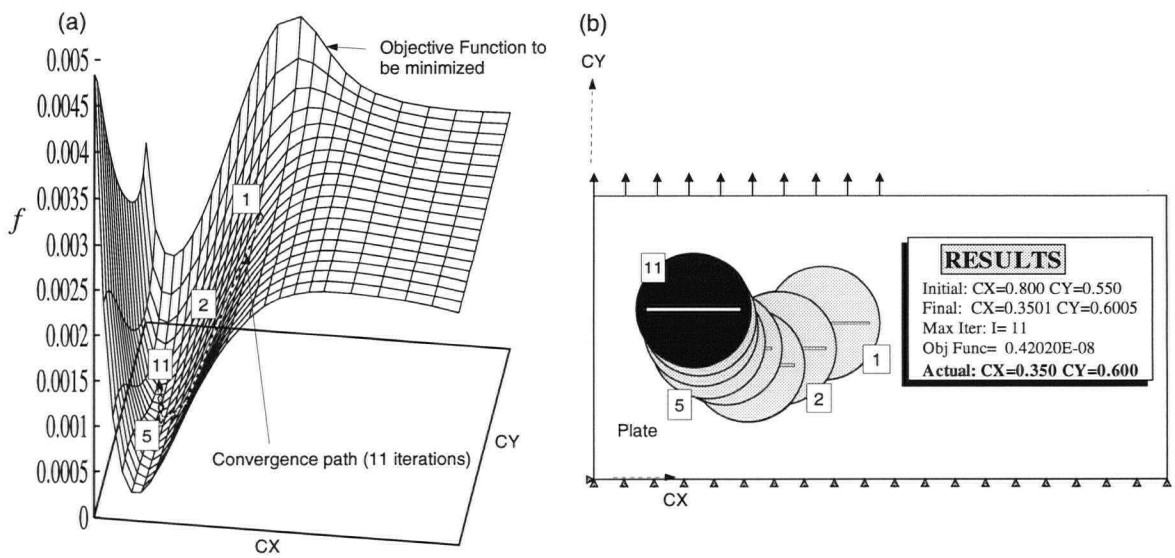

Figure 3.8: Convergence process for a plate containing a through-thickness crack: (a) Objective function surface plot with convergence path superimposed; (b) Plate and crack with iteration positions.

To further study the convergence process, five additional problems were executed,

each with different starting values for C_X and C_Y. Three of the problems had guess values for C_X which were less than 1 m (left half of the plate) and the solution converged to the global minimum. The other two problems had initial C_X values greater than 1 m (right side of the plate) and converged to the local minimum at C_X=1.75 m and C_Y=0.25 m (right bottom corner of the plate). Again, both results should be considered successful solutions.

For the complete study, the parameter vector was extended to include θ and R, as well as C_X and C_Y. In addition, to further test the analysis procedure, the rectangular plate was replaced by a square plate, and the uniformly distributed load was replaced by a ramped load that was applied to the entire upper edge of the plate. The convergence analysis for this model is displayed in Figure 3.9. Again, the figure includes a numerical summary which contains the guess values, final solution, number of iterations, objective function value at the solution, and the true design variable values at the global minimum. Considering the summarized results, the analysis procedure obtained an accurate solution for the crack identification model.

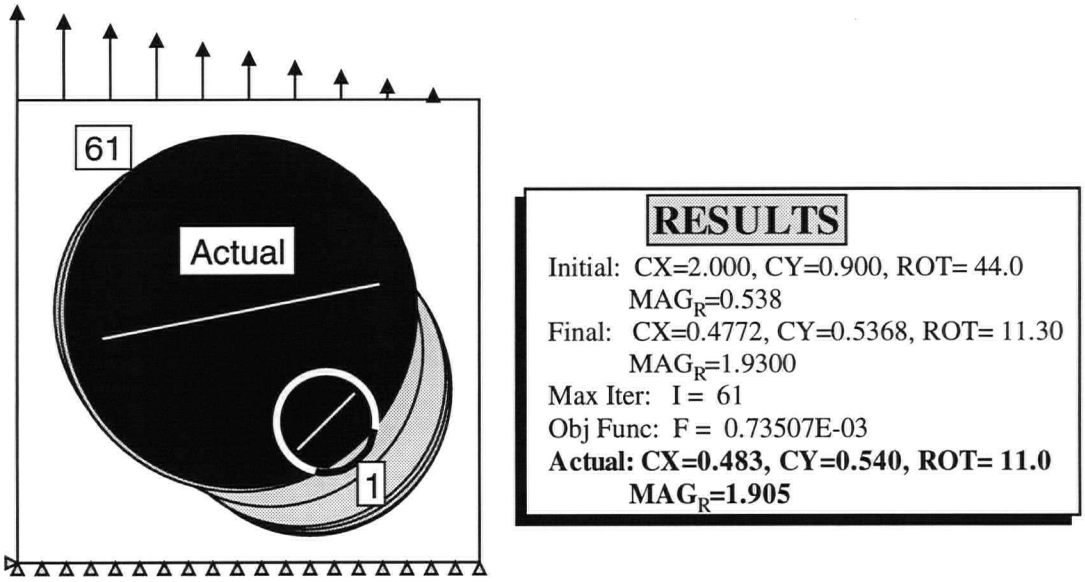

Figure 3.9: Convergence process for the crack identification model.

3.1.3 Numerical Considerations

Three numerical aspects are unique to, and essential for, the analysis procedure presented in the previous section. The necessity of these numerical components became apparent during the extended numerical studies. These unique aspects are discussed in the following subsections.

Line Search Modification

During the numerical study, the analysis of certain problems failed as a result of the inclusion moving outside the domain of the plate in spite of having the correct constraints. After investigation, it was discovered that this behavior was caused by the line search subroutine of NLPQL. From the previous theory, NLPQL calculates a new design point $\mathbf{x}^{(k+1)}$ by determining a search direction $\mathbf{d}^{(k)}$ and a positive scalar step length α_k ($\mathbf{x}^{(k+1)}=\mathbf{x}^{(k)}+\alpha_k\mathbf{d}^{(k)}$). The calculation of the line search is based on the augmented Lagrangian type line search or merit function. During the line search procedure α_k is initially assigned a value of unity and the objective function value is evaluated at this location. The objective function value is used to test whether the merit (or descent) function is satisfied. If it is, the step length (α_k=1) and the objective function value are used to obtain a quadratic fit of the merit function in order to calculate the new design point, otherwise, α_k is reduced until the merit function is satisfied. The important detail to note is that an objective function value is required each time α_k is updated. Therefore, if $\mathbf{d}^{(k)}$ is in the direction of a constraint, the initial step length of unity may result in one or more of the design variable values residing outside the feasible region. The line search method does consider the upper and lower bounds on each design parameter and

will not attempt to step outside these values, but the prescribed constraints are not taken into consideration. This does not pose a problem when analytic functions are evaluated because the objective function can still be calculated outside the feasible region. However, for FE problems, where the constraints represent physical restrictions on the model geometry, an objective function value does not exist outside the feasible domain. For subsurface cavity detection problems this is equivalent to having the inclusion outside the boundaries of the plate, which is meaningless. The reason this problem did not arise during the initial numerical study is evident from the objective function surface plots. The relatively large objective function values around the boundary of the feasible region always resulted in the descent direction pointing away from the constraints. However, with the greater number of variables for the extended study, the descent direction frequently pointed towards a constraint, which occasionally caused an error during the line search process. To solve this problem, the current search direction is retained, but its length is altered so that the first step always remains inside the feasible region. The steps for accomplishing this are as follows:

1) On the first step of the line search, check the value of all the constraints.

2) If all the constraints are greater than or equal to zero, do not modify the line search procedure.

3) Otherwise, reduce the value of alpha by some small percentage (0.001% for example) and recheck the constraints. Repeat this until all constraint values are greater than or equal to zero.

NLPQL's line search subroutine was altered to incorporate these modifications. A subroutine was also added to the main program to support these changes.

Insensitivity of the Analysis to the Inclusion Rotation

For certain types of NLP problems, changing a particular design variable may have an insignificant effect on the objective function value relative to other design variables. In this case, the analysis is considered to be insensitive to that design variable. This insignificance is mathematically represented by a small value of the derivative of the objective function with respect to the design variable. As a result, the NLP process will alter this variable very little during the analysis and will find the best solution using the remaining variables.

For both the generalized and the crack identification models, the rotation of the superelement had little effect on the objective function value compared to the other design variables. As a result, the procedure converged to the "best" possible solution without changing the rotation (changes of less than 5° were seen). However, if the problem is altered such that θ is the only design variable, the dominating affects of the other design variables are eliminated and the solution converges to the correct value of θ. Therefore, the solution procedure can be partitioned into two separate inverse analyses per iteration; one to solve a complete analysis for the rotation and the other to solve another full analysis for the remaining variables. This process is repeated, using the previous solution for each variable as the initial guess for the following iteration, until the difference in design variables between two consecutive solutions becomes negligible. This can be accomplished by pre-defining a convergence criteria with respect to the design variables, e.g. $|(\mathbf{x}^{(k+1)}-\mathbf{x}^{(k)})/\mathbf{x}^{(k)})|<0.01$].

Accounting for Changes to the Radius of the Inclusion

To determine the correct radius of the inclusion R, while still using substructuring techniques, a special approach to creating the finite element model is required. Recall that for

substructuring to be of benefit, the generation pass to create the superelement should be executed only once (i.e. the superelement should not change during the analysis). This will not be the case if the radius of the inclusion is altered. Therefore, instead of actually varying R, a scale factor representing the change of R from its original size is used as a design variable. Using this approach, a change in the superelement radius can be simulated by scaling the regular elements and loads of the FE model by a magnification factor, mag_{PL} (*mag*nification of the *PL*ate). Consequently, instead of varying R, mag_{PL} is used as a design variable and is defined as the inverse of the scaling factor for the variation of R. Since the analysis is linear, an equivalent model can be obtained by keeping R constant and multiplying the dimensions of the plate and loads by $1/(\text{scale factor})_R$. Note that to apply this scaling method, the dimensions of the plate can no longer be defined in terms of the global Cartesian system; instead the vertices of the plate must be defined with respect to a local coordinated system at the center of the inclusion. Figure 3.10 illustrates the difference between varying the inclusion radius when using substructuring as opposed to simply using regular elements.

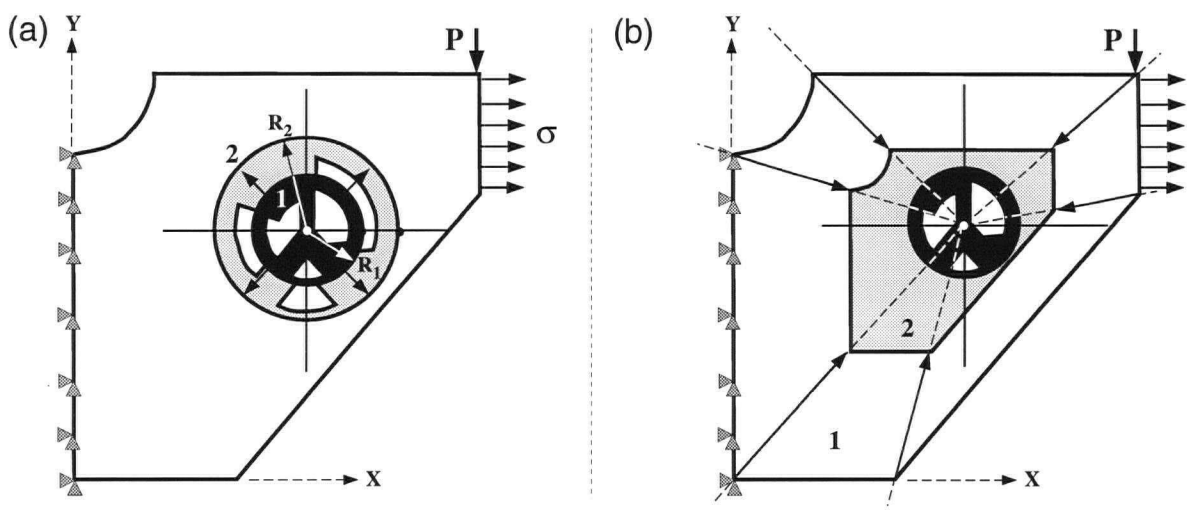

Figure 3.10: Variation of inclusion radius using: (a) "regular" elements; (b) a superelement.

Once the solution for mag_{PL} is obtained, the required radius of the inclusion can be calculated from the expression $R_{INCLUSION}=(1/mag_{PL})*R_{SE}$, where R_{SE} is the radius of the superelement when it was created. Similarly, the material properties of the superelement cannot be altered during the analysis. Therefore, the variation of E is simulated by scaling the Young's modulus of the plate by a magnification factor mag_E, which is defined as the inverse of the scaling factor for the variation of the Young's modulus of the inclusion. Again, once mag_E is obtained, the required Young's modulus for the inclusion can be calculated from the expression $E_{INCLUSION}=(1/mag_E)*E_{SE}$, where E_{SE} is the Young's modulus of the superelement when it was created. The Young's modulus and radius of the inclusion for both models were obtained using the above magnification factors.

3.1.4 Discussion

The results of the numerical examples demonstrate that the interior geometry and material properties of an inaccessible region can be determined accurately and efficiently using the proposed analysis procedure. Incorporating substructuring into the analysis procedure has proven to enhance the analysis procedure considerably. The benefits of using substructures during the FE portion are evident when taking into account the large number of objective function evaluations required for the analysis. For each iteration, partial derivatives of the objective function with respect to each design variable are required. Therefore, in addition to the initial forward FE problem, five other FE problems must be solved to calculate the derivatives using a forward difference scheme. Additional function evaluations may also be required during the line search part of the solution. For problems where the inclusion is

relatively large, the number of DOF of the finite element model can be substantially reduced with the use of substructuring. For some models, computational saving of roughly 50% were achieved.

Additional affects on the solution procedure have been considered by other researchers. Altering various system parameters, such as the number of sensor locations and their distribution and mesh density, have been examined. In addition, inverse problems are inherently ill-posed. This means that a solution may not be unique, may not exist, and may be numerically unstable if errors are introduced into the objective function. This issue has prompted researchers [5,7] to study the effects of adding a random error to the reference displacements to simulate experimental noise. Given the nature of inverse parameter identification problems, the results of these studies are highly problem-dependent and the conclusions of limited generality. As a result, the effects of changing these various system parameters were not included in the scope of this research. Also, the studies conducted using random input error were still based on a deterministic view of the system. In a strict sense, the stochastic description of the input data requires that the problem be formulated in a probabilistic manner. Methods such as the maximum likelihood principle [65], have been proposed (although not with specific reference to subsurface flaw detection) by researchers to incorporate random experimental noise. Recently, Fadale et al. [66] have developed a new objective function, which accounts for the stochastic nature of the experimental reference data and of the design parameters (the actual parameters can only be measured within a certain accuracy).

Incorporate probabilistic theory into the inverse analysis procedure could be the objective of future work. Research could also be conducted to develop a library or database of

inclusion types and geometries. This would allow multiple situations (multiple defects) to be modeled internally by the program and the solution which best matched the experimental data would represent the internal conditions of the structure. Three dimensional geometries, nonlinear material and geometric behavior, and anisotropic materials could be considered.

In addition, if a large number of design variables are required to characterize a complicated inclusion, the potential of the optimization process to converge to a local minimum increases. As a result, to aid in detecting the globally optimum solution, the analysis should be conducted using multiple guess values. Quasirandom sequence generators [67] could be used to determine a desirable dispersion of these initial guess values throughout the feasible region.

The addition of these modifications to the theoretical study of subsurface cavity detection may aid in the future development of procedures for the inspection of actual engineering structures and components.

3.2 Crack Propagation

To verify the proposed solution procedure given in Figure 2.5, the following four finite element models, each representing an increasingly more complex fracture situations were considered: a horizontal through-thickness crack in a finite plate; an inclined through-thickness crack in a finite plate; a crack parallel to a bimaterial interface; and a transverse crack in two fiber-reinforced composite materials. The first three models were used as test cases. For these numerical studies, only one crack growth step was considered ($m_{max}=1$) since only the initial directions of crack extension are documented in the literature. For the crack growth in the two composite materials, an analytical solution does not exist and the objective of the inverse analysis is to duplicate the crack behaviors observed experimentally. Three crack growth steps are considered for both composite models and the direction of crack extension is determined at each step. The results obtained for all the numerical models are in agreement with the expected values.

3.2.1 Formulation of Nonlinear Programming Problem

For the inverse problem of crack propagation, the objective is to maximize the strain energy release rate $G(\theta)$ which can be accomplished by minimizing $1/G(\theta)$. The design variable vector consists of one element θ which is restricted by its upper and lower bounds of 180° and -180° respectively. Therefore, the standard optimization form of the problem becomes:

$$\begin{aligned} &\text{Minimize:} \quad f(\theta) = \frac{1}{G(\theta)} \\ &\text{Subject to:} \\ &-180^\circ < \theta < 180^\circ \end{aligned} \tag{3.5}$$

It should be noted that equation (3.5) is a one-dimensional unconstrained optimization problem. This type of problem is not as complex as the generalized problem defined in equation (2.12) and a number of simple algorithms are available for its solution [55]. However, NLPQL has been selected to solve equation (3.5) because of its availability [59], excellent previous performance for subsurface cavity detection problems, and its ability to efficiently and accurately solve a wide variety of optimization problems [60,61], including the one-dimensional unconstrained cases.

3.2.2 Finite Element Formulation

The finite element modelling procedure for examining crack propagation requires the same techniques used for the subsurface cavity detection study; however, substructuring is not required. The ANSYS input file for each problem in this section is capable of modelling a crack in any configuration (location or orientation) without requiring user interaction. The crack is initially assigned a finite width, then after the entire model has been automeshed, the elements along the two faces of the crack tip are modified to close the crack tip (coincident crack faces). The homogeneous models were constructed with crack tip elements encircling the entire kinked tip.

A plane strain analysis was conducted for each numerical model and all material domains were assumed to be isotropic and linearly elastic. The elastic energy of each element was extracted during the post-processing phase of the analysis and the the total strain energy of the structure was obtained by summing these values.

3.2.3 Horizontal Crack in a Finite Plate

The model depicted in Figure 3.11 consists of a two-dimensional finite width plate, which contains a straight through-thickness center crack subjected to pure mode I loading conditions.

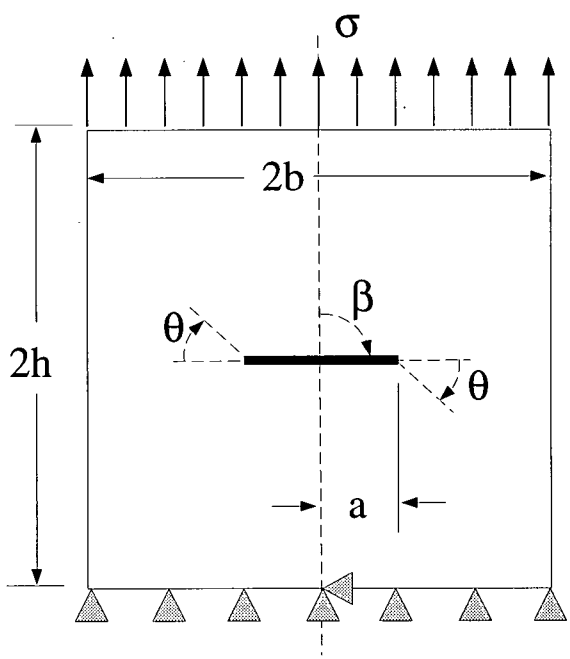

Dimensions
a = 1 [in], Δa=1/3 [in]
b = 5 [in]
h = 5 [in]
σ = 0.56419 [psi]
β = 90°

Material Properties
E = 30e06 [psi]
ν = 1/3

Figure 3.11: Center cracked plate.

The finite element model was constructed using the data in Figure 3.11 and was automatically meshed using 8-noded isoparameteric elements and nine singular elements surrounding each crack tip. Figure 3.12 shows the finite element meshes of the entire model

and the crack tip in its initial kinked configuration. Linear elastic material behavior and plane strain conditions were assumed.

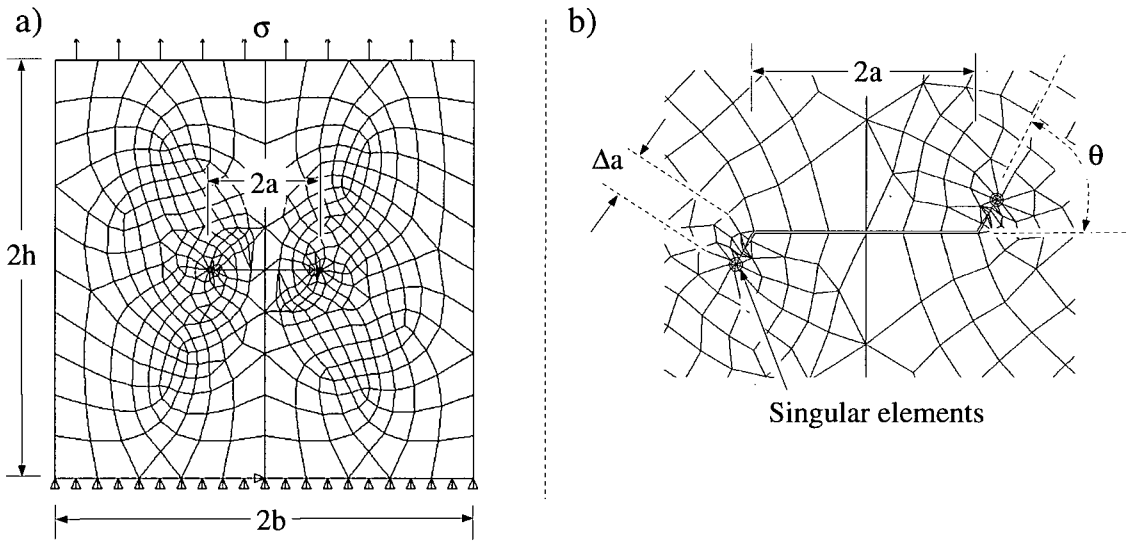

Figure 3.12: Finite element meshes for: (a) horizontal crack model with original crack configuration; (b) local kinked crack configuration (θ=60°).

As required by the solution procedure, the finite element model was designed so that the crack could be extended by a small amount Δa in any direction θ and the total strain energy/energy release rate obtained for the given configuration. To graphically visualize the objective function (actually, the inverse of the objective function), a polar plot of the energy release rate as a function of the the crack tip angle G(θ) was created prior to running the inverse analysis. This curve was constructed by varying one of the extended portions of the crack from -90° to 90° in increments of 1°, while simultaneously rotating the other tip from 90° to -90°, and obtaining the strain energy at each kink angle. As discussed earlier, the value of θ associated with the maximum value of the strain energy is equal to the value associated with the maximum value of the strain energy release rate; therefore, the solid curve given in

Figure 3.13 is referred to as G(θ) even though the actual curve is U(θ). G(θ) is plotted in Figure 3.13, as opposed to the actual objective function 1/G(θ), to stay consistent with the fracture criterion, which states that the maximum value of the energy release rate be determined (not the minimum of its inverse). For this model, G(θ) was plotted instead of

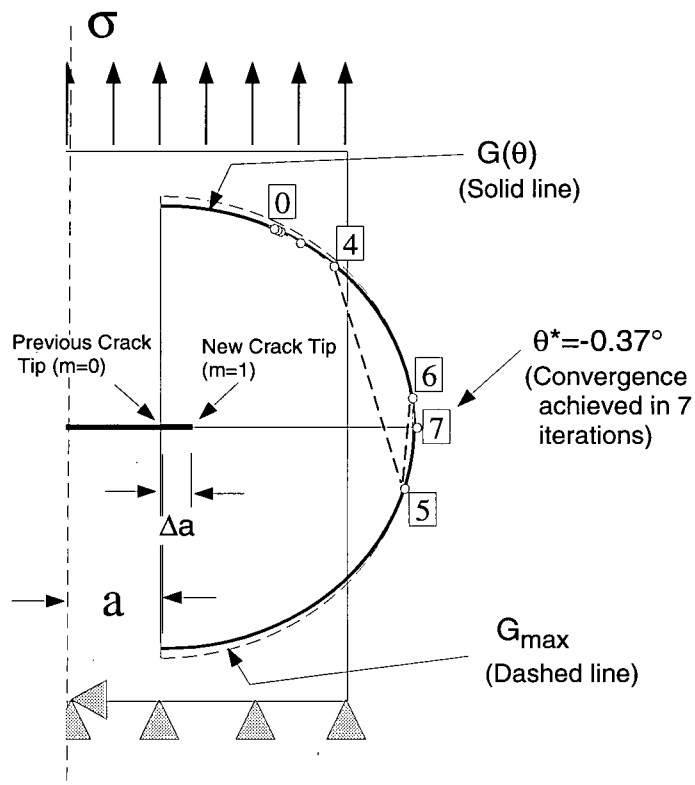

Figure 3.13: Polar plot of G(θ) with the convergence process superimposed.

$G(\theta)/G_c$ because the material is entirely homogeneous; thus, the direction of crack growth is independent of the magnitude of G_c. The dashed line in Figure 3.13 represents a constant radius equal to G_{max} and is used strictly for reference purposes. G(θ) values appearing inside the dashed line are less than G_{max}. The hollow circles superimposed on the solid line are the G(θ) values calculated at each increment (0 to 7) of the optimization algorithm as it progressed from an initial guess value of $\theta^{(0)}_1 = 60°$, towards a convergent solution of

θ^*_1=-0.37°. This solution is in excellent agreement with the self-similar crack growth (θ=0°) predicted theoretically [25] and observed experimentally [63] for mode I loading conditions.

3.2.4 Inclined Crack in a Finite Plate

To study the problem of crack growth under mixed mode conditions (mode I & II), the previous model was altered by rotating the center crack 40° from the horizontal; see Figure 3.14.

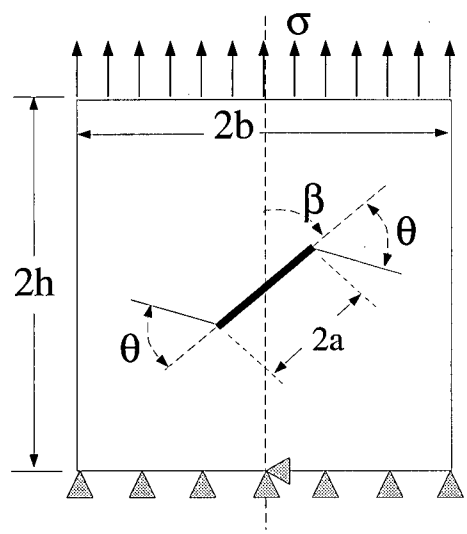

Dimensions
a = 1 [in], Δa=1/3 [in]
b = 5 [in]
h = 5 [in]
σ = 0.56419 [psi]
β = 50°

Material Properties
E = 30e06 [psi]
ν = 1/3

Figure 3.14: Center cracked plate containing an inclined crack.

Again, to obtain a graphical representation of G(θ), one crack tip was rotated from -90° to 90° (with respect to the horizontal direction) while the other tip was simultaneously rotated from 90° to -90°. G(θ) and the reference curve G_{max} are plotted in Figure 3.15. In the homogeneous material, the crack is assumed to propagate in a self-similar manner and a starting value of $\theta^{(0)}_1$=0° was supplied to the optimization algorithm. The value of G(θ) calculated by NLPQL at each iteration, starting from the initial value to the globally optimum

value, are displayed in Figure 3.14. A convergent solution of θ^*_1=46.4° was obtained in 7 iterations.

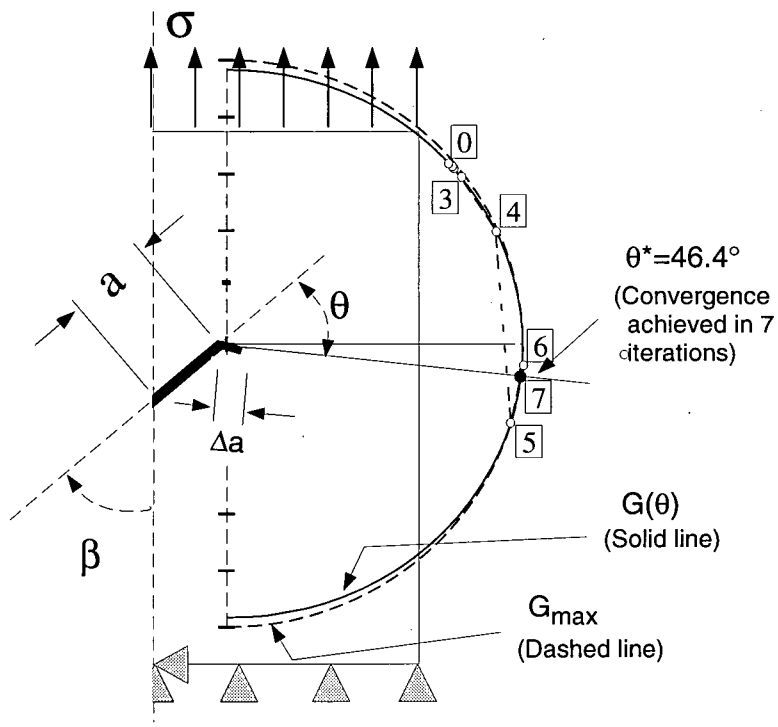

Figure 3.15: Polar plot of G(θ) and convergence process of the inverse analysis.

The theoretical solution to this problem varies slightly depending on which fracture criterion is adopted. For the particular case of an inclined crack in a finite width plate, the initial crack growth angle can be obtained from the maximum tangential stress theory by determining θ^* from the following expression [25]:

$$\sin\theta^* + (\cos\theta^* - 1)\cot\beta = 0 \ , \quad \beta \neq 0 \tag{3.6}$$

For β=50°, the value of θ^*= 50.2° is obtained from equation (3.6).

If the minimum strain energy density theory is chosen as the crack growth criteria, the initial direction of crack extension can be obtained from [34]

$$((3-4\nu)-1)\sin(\theta^*-2\beta) - 2\sin(2(\theta^*-\beta)) - \sin 2\theta^* = 0 \ , \quad \beta \neq 0 \tag{3.7}$$

The predicted angle of crack extension from equation (3.7) is θ^*=49.5°.

Huyashi and Nemat-Nasser [44] determined an analytical expression for the energy release rate of a inclined crack with a kinked tip in an infinite medium under plane strain conditions. The angle of crack extension was numerically evaluated by solving two systems of integral equations and by applying the maximum energy release rate criterion. A linear interpolation of the tabular results presented in [44] gives an initial crack growth direction (for β=50°) of approximately 53.3°. Finally, the average of four experimental tests conducted by Sih [34] on center cracked plexiglass plates (β=50°) predicted an initial crack growth direction of 51.6°. The solution of the inverse analysis θ^*_1=46.4° is in agreement with these theoretical and experimental values.

3.2.5 Interfacial Crack

The next logical progression towards studying the general behavior of crack growth in a heterogeneous domain, is to examine the specialized case of crack growth parallel to a bimaterial interface. The model and numerical data for the finite element analysis used to study this problem are shown in Figure 3.16. This model is composed of E-glass bonded to a polyester resin and contains a single crack tip which is located at the center of the plate. As before, the function $G(\theta)$ was obtained by varying the crack tip angle. With the dissimilar critical energy release rates of the two materials, $G_c^{(1)} \neq G_c^{(2)}$, the function $G(\theta)/G_c^{(i)}$ must be maximized to determine the direction of crack growth. This function becomes discontinuous at θ=0°, as seen in Figure 3.17, and the maximums of three separate regions θ>0°, θ<0° and θ=0° need to be considered. The interface between the two materials was assumed to be

perfectly bonded ($G_c^{(int)}=G_c^{(2)}$) and is represented by the solid dot at $\theta=0°$. The hollow dot in Figure 3.17 indicates that $G(\theta)/G_c^{(1)}$ approaches $\theta=0°$, but is undefined at $\theta=0°$. For the inverse analysis, $\theta^{(0)}=0°$ was used for the initial starting point. The maximum value of $G(\theta)/G_c^{(2)}$ and its corresponding crack growth angle $\theta^*=45.8°$ were achieved in 5 iterations. Referring back to the solution procedure given in Figure 2.4, the algorithm terminated after locating this maximum because $G_c^{(Resin)} < G_c^{(E\text{-}glass)}$.

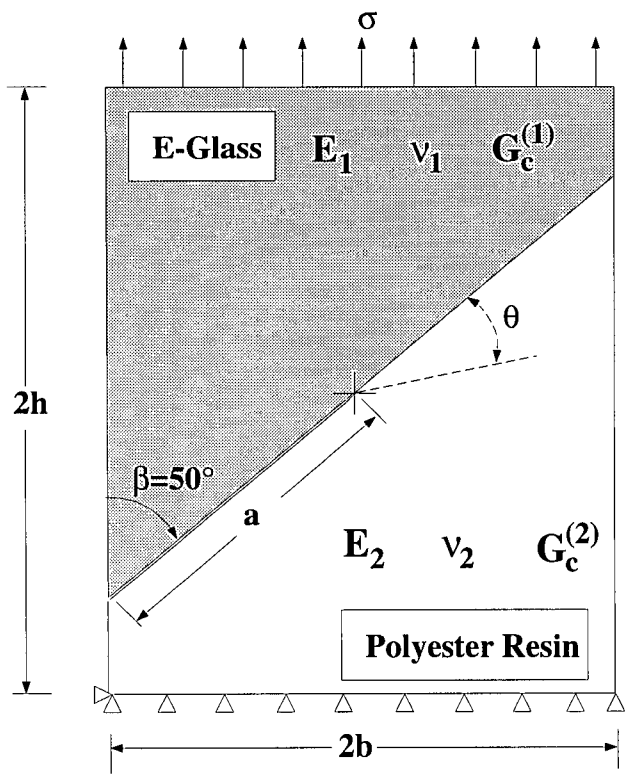

Dimensions

$a = b/\sin(\beta)$ [m], $\Delta a=a/4$ [m]

$b = 5$ [m], $h = 3$ [m]

$\sigma = 1000$ [N/m^2]

$\beta = 50°$

Material Properties

1. E-Glass:
   $E_1=76$ [GN/m^2]
   $\nu_1=0.22$, $G_c^{(1)}=20$ [J/m^2]
2. Polyester Resin :
   $E_2=3.25$ [GN/m^2]
   $\nu_2=0.38$, $G_c^{(2)}=10$ [J/m^2]

Figure 3.16: Inclined crack tangential to a bimaterial interface.

To compare the numerical solution with a value presented in the literature, the bimaterial constant ε for this model is required. This constant is a function of the shear modulus μ_j and the Poisson's ratios ν_j (j=1,2) of the two materials and is defined mathematically by the

following equation [40]:

$$\varepsilon = \frac{1}{2\pi}\ln\left\{\left(\frac{\kappa_1}{\mu_1}+\frac{1}{\mu_2}\right)/\left(\frac{\kappa_2}{\mu_2}+\frac{1}{\mu_1}\right)\right\} \tag{3.8}$$

where Muskhelishvili's constant κ_j (j=1,2) is defined as κ_j=3-ν_j for plane strain conditions. For the materials used for this numerical study, ε=0.054. Using the maximum tangential stress criterion, Meyer et al [40] present a graph of the predicted kink angle vs. $\tan^{-1}(K_{II}/K_I)$, where K_{II} and K_I are mode II and mode I stress intensity values associated with the original crack tip. Multiple curves are plotted to include the effects of varying ε from 0 to 0.175. From these curves and a value of $\tan^{-1}(K_{II}/K_I)\approx 2\pi/9$, the initial value of crack extension is approximately 44°, which is in good agreement with the solution obtained from the inverse analysis.

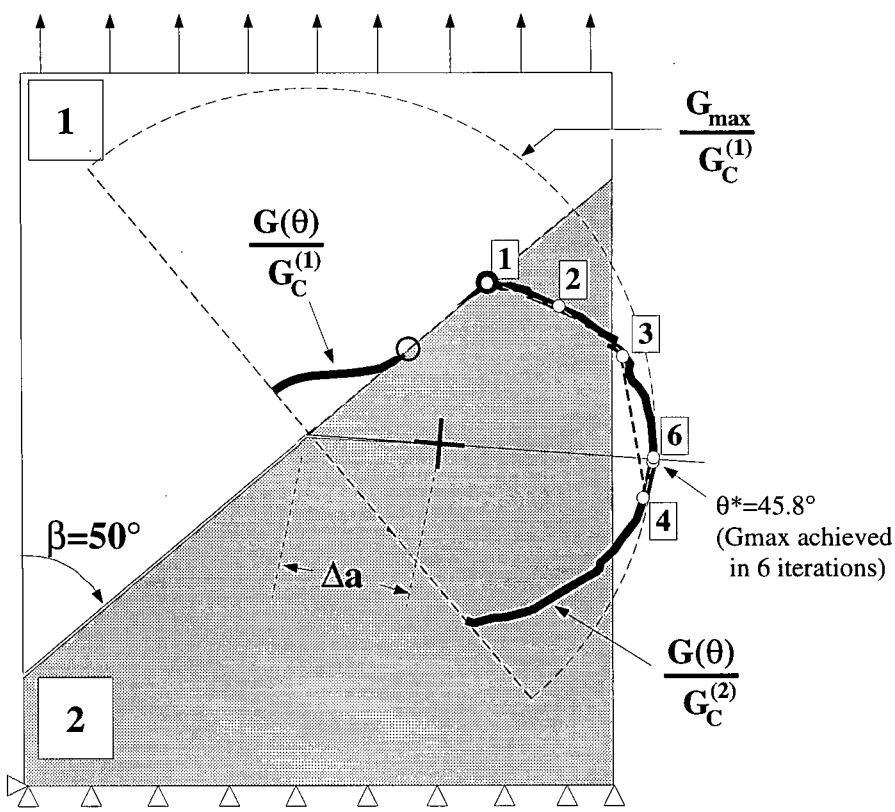

Figure 3.17 Polar plots of $G(\theta)/G_c^{(i)}$ and iterations of the optimization algorithm for an inclined crack along a bimaterial interface.

3.2.6 Transverse Cracks in Fiber Reinforced Composites

Glass Fiber-Polyester Resin Lamina

Microscopic studies of the fracture of composite laminae show that transverse cracks can nucleate in regions of dense fiber packing and can continue to propagate through the laminae. Figure 3.18 shows the experimentally observed behavior of a crack propagating in the transverse direction of a glass fiber-polyester resin lamina.

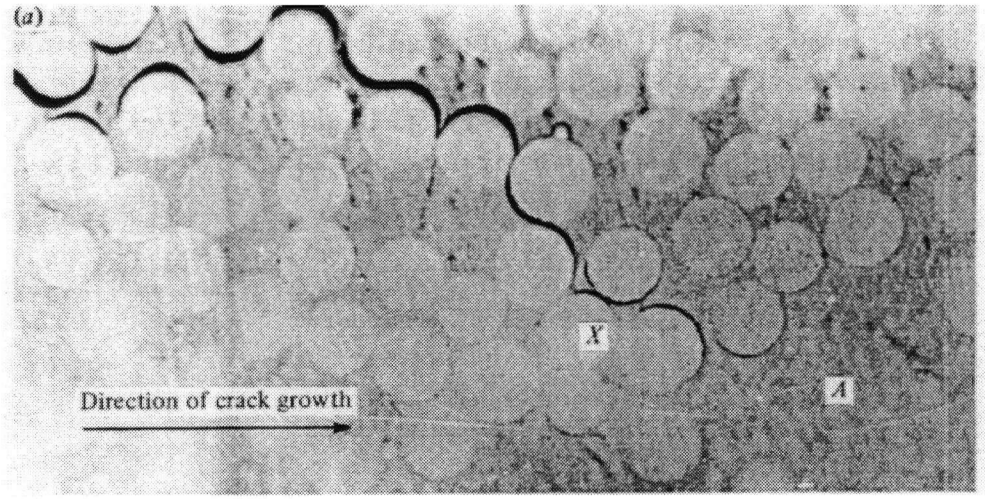

Figure 3.18: Experimentally observed propagation of a transverse crack in a glass-polyester resin lamina [68].

To apply the inverse analysis procedure to this type of problem, the model in Figure 3.19 was constructed. This model consists of a single crack that is approaching an E-glass fiber emanating from within a polyester resin matrix. The objective of the numerical study is to determine the crack growth directions for a number of increments of crack extension. To obtain the functions $G(\theta)/G_c^{(i)}$, the crack tip was varied from -70° to 90° and the strain energy of the structure was obtained at each kink angle. The $G(\theta)/G_c^{(i)}$ curves for each increment of growth are given in Figure 3.20.

For reference purposes, the polyester resin and E-glass fiber have been designated Material 1 and Material 2, respectively. As outlined in Figure 2.4, $\theta^{(0)}{}_1=0°$ was determined from the assumption of self-similar crack extension in a homogeneous domain. For subsequent iterations, a perfectly bonded interface was assumed and the corresponding $\theta^{(0)}{}_m$ values were determined from the previous increment's solution for the direction of crack growth $\theta^*{}_{m-1}$ (again, self-similar crack extension). The results for this analysis are shown in Figure 3.20.

For the first increment of crack growth, the kinked tip of the crack remained in the polyester matrix and the analysis was similar to the horizontal crack model discussed earlier. However, the effects of the stiffer E-glass fiber caused the crack growth to be deflected downward by approximately 5° from the horizontal direction. For the remaining two increments, the crack also mimicked the behavior seen experimentally (Figure 3.18) and tended to travel tangential to the material interface

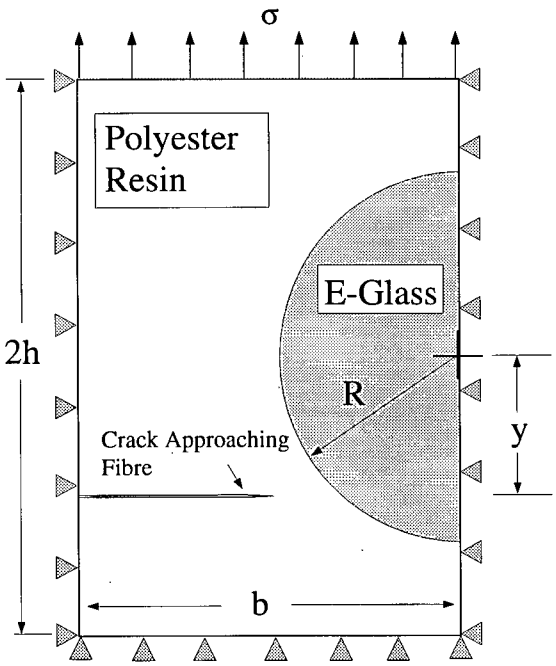

Dimensions

a = 4 [μm], Δa=1 [μm]
b = 6.2 [μm], h =4.5 [μm]
σ = 0.001 [N/m^2]
R=3 [μm]
y=√5 [μm]

Material Properties

1. Polyester Resin :
   E_1=3.25 [GN/m^2]
   ν_1=0.38, $G_c^{(1)}$=10 [J/m^2]
2. E-Glass:
   E_2=76 [GN/m^2]
   ν_2=0.22, $G_c^{(2)}$=20 [J/m^2]

Figure 3.19: Crack approaching the interface between a polyester resin and a glass fiber.

Figure 3.20 illustrates that acceptable results for each increment of crack extension were obtained using relatively few iterations.

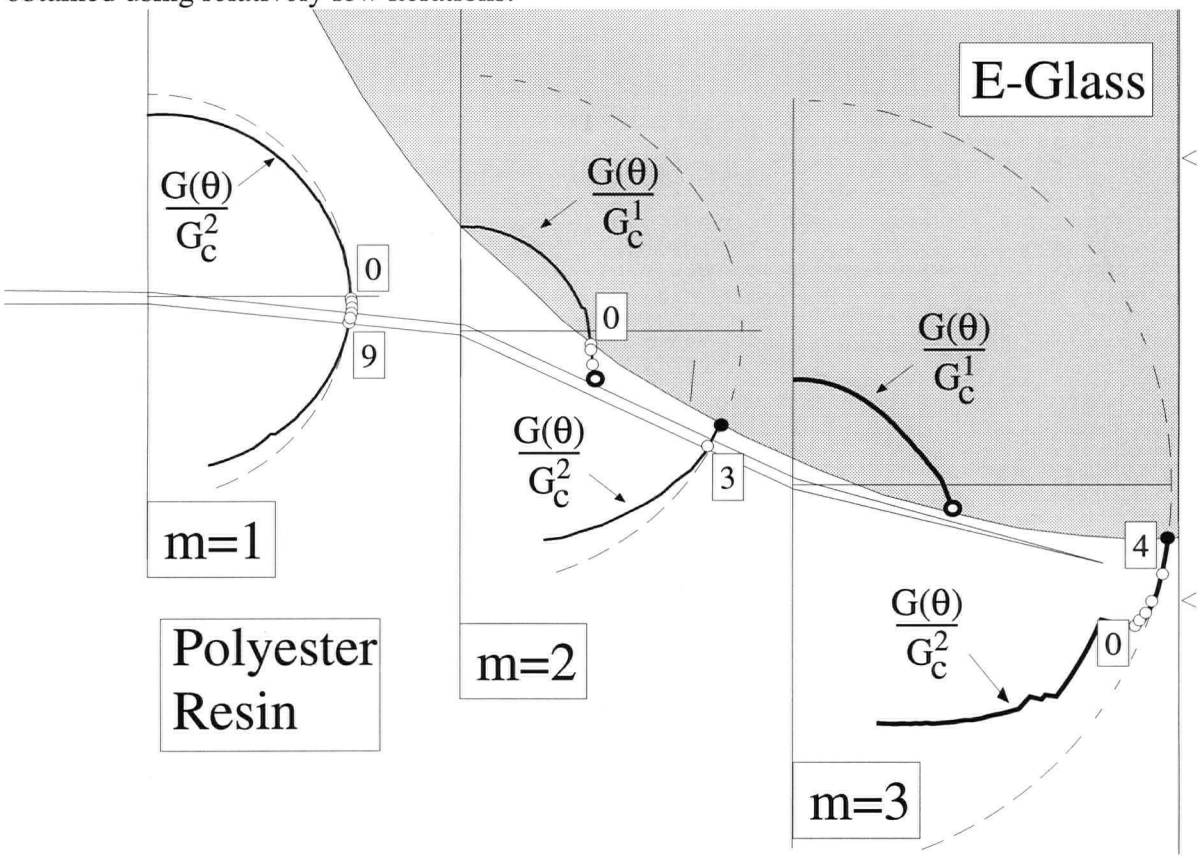

Figure 3.20: Numerically predicted crack propagation path in the transverse direction of a glass-polyester lamina. The general behavior is consistent with experimentally observed crack growth.

Glass Fiber-Aluminium Matrix lamina

In general, the crack growth behavior seen in Figure 3.18 holds when the fiber is tougher than the matrix, i.e. $G_c^{(fiber)} > G_c^{(matrix)}$. However, for materials such as metal matrix composites, the matrix may be tougher than the fiber. In this case, crack growth generally behaves as shown in Figure 3.21. The aluminium matrix is tougher than the E-glass fiber for this lamina, so consequently the crack tends to leave the matrix and propagate through the fiber.

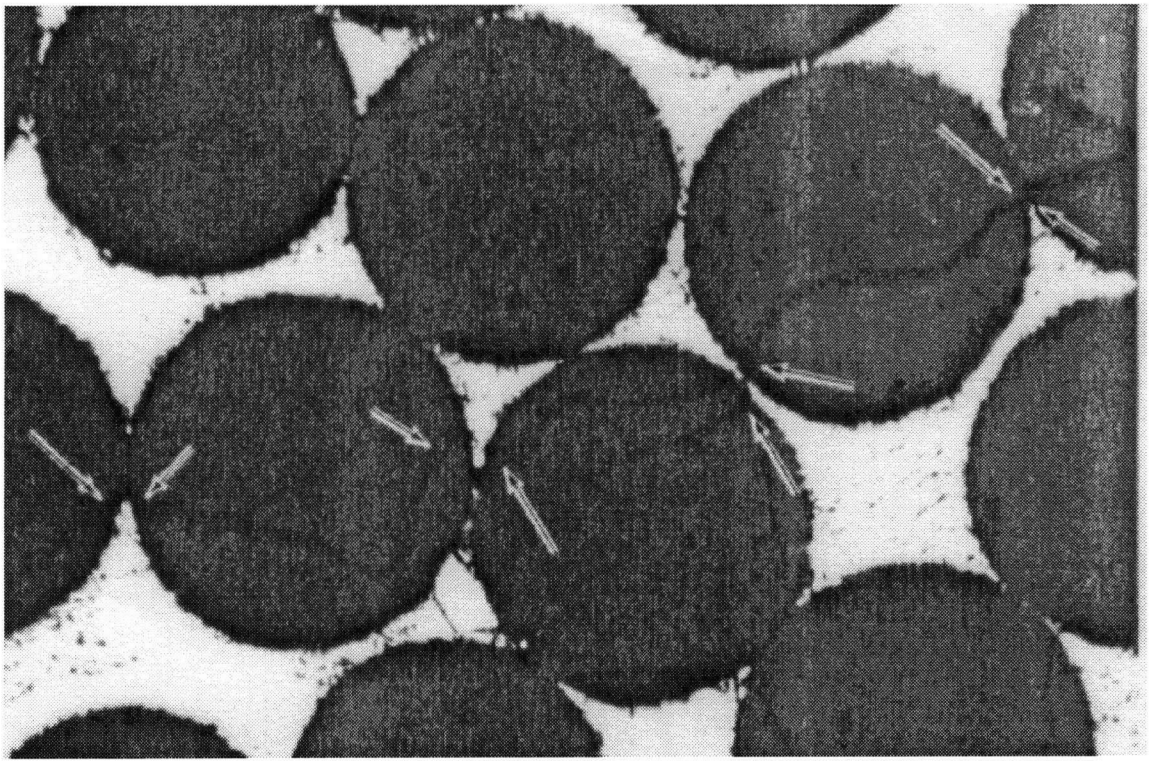

Figure 3.21: Propagation of a transverse crack in a glass fiber-Al matrix lamina [69].

To duplicate this behavior, the same model shown in Figure 3.18 was used with the matrix material changed from a polyester resin to Aluminium (6061-T6). The analysis procedure was similar to that for the glass-polyester model except that the critical energy release rate of the interface was assumed to be 20% less than that predicted by perfect bonding, i.e. $G_c^{(int)}=0.8(G_c^{(2)})$. This assumption did not affect the first or last increments of crack extension, since these two crack tips were entirely within homogeneous regions. However, for the intermediate step, the crack tip was placed tangential to the interface. The results of the inverse analysis are given in Figure 3.22. The change in matrix properties from the previous model causes the behavior of the crack to differ substantially from the results in Figure

3.20 and is more consistent with the observed behavior seen in Figure 3.21. Again, the inverse analysis produced acceptable results with relatively little computational effort.

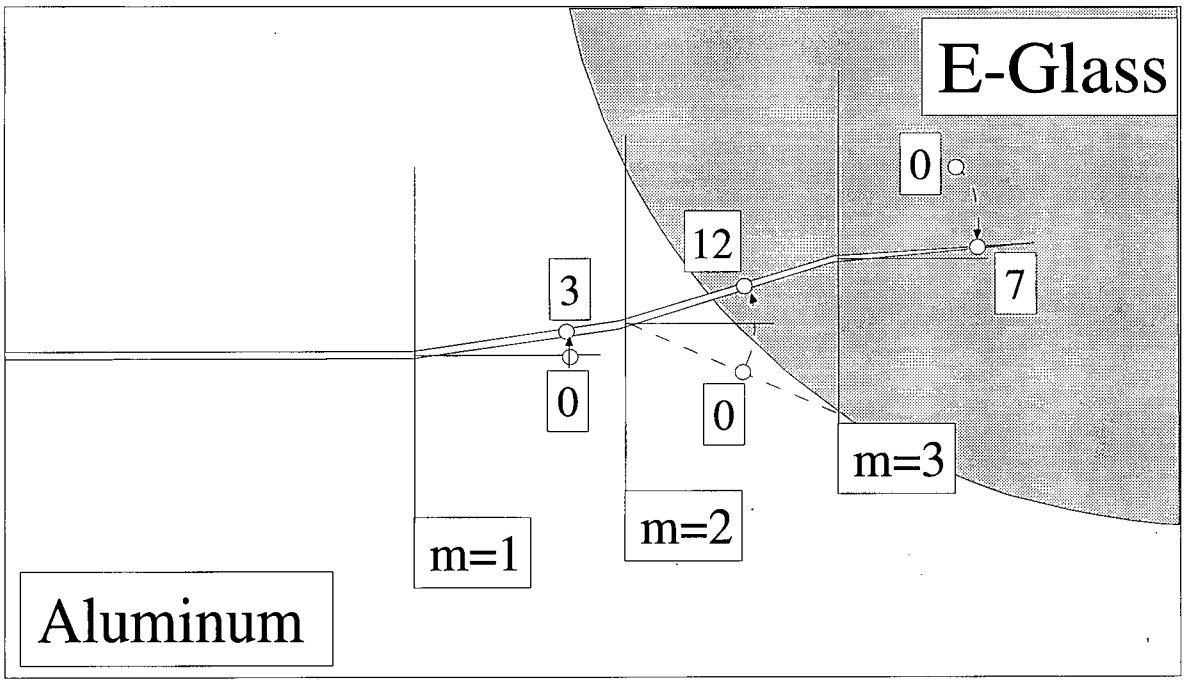

Figure 3.22: Numerically predicted crack propagation path in the transverse direction of a glass-Al lamina. The general behavior is consistent with experimentally observed crack growth.

Figure 3.23 shows the finite element representation of this model with the kinked tip at θ^*_3. Notice for this final step, where the effects of the interface start to diminish, the crack begins to resume its growth perpendicular to the applied load (pure mode I), which is the expected direction of growth in the absence of a material interface.

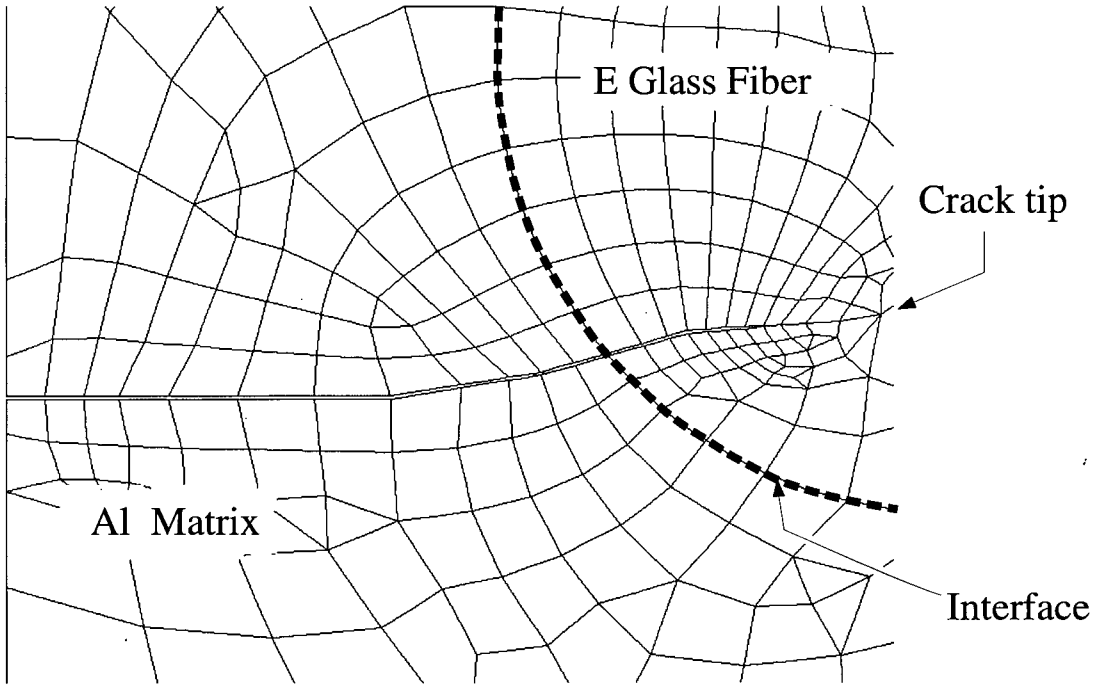

Figure 3.23: Finite element mesh of glass-Al lamina (final solution).

3.2.7 Discussion

The results of the numerical study indicate that the direction of crack growth under unimodal and mixed mode loading, as well as for homogeneous and heterogeneous materials, can be obtained efficiently and accurately using the numerical procedure presented in this paper. To ensure that the algorithm performs as intended, several modelling aspects should be considered.

The length of the crack extension Δa can affect the analysis in several ways. The smaller the value of Δa (or the larger the model), the closer the physically real situation of a continuously propagating (as opposed to discretely incrementing) crack is represented . How-

ever, as Δa becomes excessively small the difference between the maximum and minimum values of the strain energy as a function of crack tip angle, decreases. This "flattening out" of the objective function causes the values of the derivatives to decrease, which in general also decreases the rate of convergence of the nonlinear programming algorithm. In addition, the potential increases for numerical or finite element modelling errors, such as errors in derivative estimation or in automatic mesh generation.

It is well accepted [22] that crack tip elements should be used to correctly represent the singular stress/strain field in the vicinity of the crack tip. For this reason, these elements were utilized when modelling the homogeneous fracture cases. However, difficulties arose when including these elements in the bimaterial and composite models. The modelling techniques used to prevent these elements from interfering with the material interface inevitably resulted in the interface becoming slightly distorted or jagged. Since the degree of distortion varies depending on the value of θ, the objective function became quite "noisy" (non-smooth). This produced significant errors when calculating the numerical derivative of the objective function with respect to θ. Therefore, crack tip elements were not used for the inhomogeneous models, and this resulted in a much smoother and a more easily differentiable objective function. In addition, since the strain energy of the entire structure is of primary interest and not the very localized stress field around the crack tip, excluding the singular elements had a negligible effect on the objective function values.

The procedure presented here for determining the direction of crack growth in a heterogeneous domain may be extended to include dynamic or crack growth rate effects, three-dimensional crack propagation, ductile materials and multiple interacting cracks.

Chapter 4

Conclusions

Engineering structures or components can contain pre-existing flaws or defects which, under the influence of high loads, fatigue, or chemical damage, can initiate cracks and may eventually cause failure. As a result, it is beneficial to be able to nondestructively inspect a structure for subsurface flaws and to have an understanding of how internal cracks propagate under complicated loading or geometric conditions. This thesis has contributed to this understanding by presenting numerical procedures for solving inverse parameter identification problems in solid mechanics. Incorporating the finite element method and optimization techniques has proven, through numerical examples, to be an efficient and accurate means of determining the required system parameters. The specific applications of subsurface cavity detection and of crack growth through a heterogeneous domain were considered.

An economical and accurate procedure was presented for the numerical identification of subsurface flaws or cracks. The procedure is based on updating the interior geometry of a structure until the displacements calculated on the exterior of the plate match those obtained experimentally. Enhancements in robustness and computational efficiency over previously proposed numerical methods are realized through the use of finite element substructuring techniques and an efficient Quasi-Newton type optimization algorithm. Several numerical

example problems were constructed and their solutions successfully obtained using this procedure. Suggestions regarding future work in this area have also been presented. The enhancements presented in this thesis as well as these recommended modifications represent a step towards extending this analysis beyond numerical confines and towards the nondestructive evaluation of newly manufactured and in-service structures and components.

The problem of determining the direction a crack will propagate in a heterogeneous domain was also formulated using inverse methodology. This procedure is based on determining the direction of crack growth, which corresponds to the maximum normalized energy release rate of the structure, for a given increment of crack growth. Again, the procedure utilizes the finite element method and sequential quadratic programming to solve for the angle of crack extension. The procedure was applied to several numerical test cases as well as two composite laminas. The results of the study were consistent with the theoretical and experimental findings. Suggestions regarding future work in this area were also presented.

References

1. Kubo, S., Inverse Problems Related to the Mechanics of Fracture of Solids and Structures, JSME International Journel, Series I, Vol. 31, No.2, 1988.

2. Dulikravich, G.S., Inverse design and active control concepts in strong unsteady heat conduction, Appl. Mech. Rev., 41, 270-277, 1988.

3. Beck, J.V., Blackwell, B., and St. Clair, Jr. C.R., Inverse Heat Conduction: Ill-Posed Problems, Wiley-Interscience, New York, 1985.

4. Corcoran, P.J., Configuration Optimization of Structures, International Journal of Machanical Sciences, Vol. 12, pp. 459-462, 1970.

5. Schnur, D. S., Zabraras, N., Finite Element Solution of Two-Dimensional Inverse Elastic Problems using Spatial Smoothing, Int. Journal for Num. Methods in Eng., Vol. 30, 57-75 (1990).

6. Schnur, D. S., Zabraras, N., An Inverse Method for Determining Elastic Material Properties and a Material Interface., Int. Journal for Num. Methods in Eng., Vol. 33, 2039-2057 (1993).

7. Hsieh, S., and Mura, S. (1993). "Nondestructive cavity identication in structures.", Int. J. Solids and Struct., 30(12), 1579-1587.

8. Maniatty, A., Zabaras, N., Stelson, K., Finite Element Analysis of Some Inverse Elastic Problems, Journal of Engineering Mechanics, Vol. 115, No. 6, June, 1989.

9. Tanka, M., Nakamura, M., Nakano, T., and Ishikawn, H., Identification of Defects by the Elastodynamic Boundary Element Method Using Noisy Additional Information, Boundary Elements III.

10. Tanka, M., Masuda, Boundary element method applied to some inverse problems, Engineering Analysis, Vol. 3, No. 3, 1986.

11. Kassab, A.J., Moslehy, F.A., Daryapurkar, A., Inverse eleastostatics boundary element approach applied to nondestructive evaluation, Boundary elements XV, Vol. 1, 261-273, 1993.

12. Mellings, S.C., Aliabadi, M.H., Crack Identification using inverse analysis, Boundary elements XV, Vol. 2, 387-398, 1993.

13. Iwamura, Y. and Miya, K., Numerical approach to the inverse problem of crack shape recognition based on the electrical potential method, IEEE Transactions on Magnetics, Vol. 26, No. 2, 618-621, 1990.

14. Ratajeeran, S., Hoole, H., Subramanian, S., Saldanha, R., Coulomb. J.L., Sabonnadiere, J.C., Inverse Problem Methodology and Finite Elements in the identification of Cracks, Sources, Materials, and their

Geometry in Inaccessible Locations, IEEE Trans. on Magnetics, Vol. 27, No.3,1991.

15. Bui, H.D., Inverse Problems in the Mechanics of Materials: An Introduction, CRC Press, Inc., 1994.

16. Shanyi, D. and James, D.L, Finite Element Analysis of slow stable crack Growth, Engineering Fracture Mechanics, Vol. 16, No. 2, pp. 229-245,1982.

17. Shan, G.X., Kolednik, O., Fischer, F.D., and Stuwe, 2D Model for Numerical Investigations of stable crack growth in Thick Smooth Fracture Mechanics Specimens, Engineering Fracture Mech., Vol.45, No.1,pp. 99-106,1993.

18. Hoff, R., Rubin, C.A., and Hahn, G.T., A New Finite-Element Technique for Modelling Stable Crack growth, Eng. Fracture Mech., Vol.23, No.1,pp.105-118, 1986.

19. R.H. Dodds, Jr, M. g and T.L. Anderson, Numerical Procedures to model Ductile crack extrension, Eng. Fract. Mech., 46, 2, 253-264, 1993.

20. Miyazaki, N., Nakagaki, M., Sasaki, T., Sakai, T., and Munakata, T., Finite Element Analysis of Stable Crack Growth in Inhomogeneous materials, JSME Int. J., series A, Vol. 36, No.4, 1993.

21. Nishioka, T., Stonesifier, R.B., and Atluri, S.N. An evaluation of several moving singulity Finite element models for fast Fracture analysis, Eng. Fract. Mech., 15, Vol 1-2, 205-218, 1981.

22. H.Liebowitz and E.T. Moyer, Jr, Finite Element Methods in Fracture Mechanics, Comp. & Struct.,31,1,1-9,1989.

23. Anderson, H., The steadily growing, elastic-plastic crack tip in a finite element treatment, Int. J. Fracture, Vol. 9, pp. 231-233, 1973.

24. Mahanty, D.K. and Maiti, S.K., Experimental and Finite Element studies on mode I and mixed mode (I & II) stable crack growth, Engineering Fracture Mechanics, Vol. 37, No. 6, pp. 1237-1275, 1990.

25. Erdogan, F. & Sih, G.C., On the Crack Extension of Plates under plane loading & Transverse Shear, J. Basic Eng, 85, 519-527, 1963.

26. H.Feng, J. Zhang and J. Rohde, crack surface relative displacement analysis of mixed-mode Fracture Mechanics Problems, Eng. Fract. Mech. Vol 36, 6, 971-978, 1990

27. Chow, C.L. and Lau, K.J., Finite element Analysis of Cracked Bodies to Determine Stress Intensity Factors, Journal of Strain Analysis, Vol. 11, No. 1, pp. 18-24,1976.

28. Eftis, J & Subramon, The Inclided Crack Under Biaxial Load, Fracture Mechanics, 10, 43-67, 1978

29. Williams, G. & Ewing, P. D, Fracture under Complex Stress - The angled Crack Problem, Int. J. Fract. Mech, 441-446,1972

30. Sih, G. C. & Barthelemy, .B. M., Mixed Mode Fatigue Crack Growth, Eng. Fract. Mech, 13, 439-451, 1980

31. Tanaka, K., Fatigue Crack Propagation from a Crack Inclined to the Cyclic Tensile Axis, Eng. Fracture Mech., Vol. 6, pp. 493-507, 1974.

32. Chiu, S.T. and Lia, A.F., Mixed-Mode Fracture of Shear Panels- A Finite Element Analysis, Mechanics of Crack Growth, ASTM STP 590, American Society for Testing Materials, pp. 263-280, 1976.

33. Swedlow, J.L., Criteria for Growth of the Angled Crack, Cracks and Fracture, ASTM STP 601, American Society for Testing Materials, pp. 506-521, 1976.

34. Sih, G. C., Strain Energy Density Factor Applied to Mixed Mode Crack Problems, Int. J. Fracture, 11, 305-321, 1974.

35. Nuismer, R.J., An energy release rate criterion for mixed mode fracture, Internation Journal of Fracture, Vol.11, No.2, pp. 245-250, 1975.

36. Linnig, W., Some aspects of the prediction of fatigue crack paths, ESIS 14 (Edited by H.P. Rossmanith and K.J. Miller), Mechanical Engineering Publications, London, pp. 201-215,1993.

37. Pook, L.P., A finite eleemnt analysis of the angle-crack specimen, ESIS 14 (Edited by H.P. Rossmanith and K.J. Miller), Mechanical Engineering Publications, London, pp. 285-302,1993.

38. Griffith, A.A., The phenomena of rupture and flow in solids, Phil. Trans. R. Soc., pp. 163-198, 1921.

39. Rice, J. R., Elastic Fracture Mechanics Concepts for Interfacial Cracks, ASME Journal of Applied Mechanics, Vol. 55, pp. 98-103, 1988

40. Meyer, M., Schmauder, S., and Elssner, G., Mixed-mode fracture investigations of interface cracks in dissimilar media, ESIS 14 (Edited by H.P. Rossmanith and K.J. Miller), Mechanical Engineering Publications, London, pp. 303-318,1993

41. Kishimoto, K. and Aoki, S., Finite element analysis on mixed mode fracture, Mixed-Mode Fatigue and Fracture, ESIS 14 (Edited by H.P. Rossmanith and K.J. Miller), Mechanical Engineering Publications, London, pp. 267-284,1993

42. Dreirer, G., Schmauder, S., and Elssner, G., Propagation and fracture energy of interface cracks in elastically similar brittle materials under mixed-mode loading conditions, Mixed-Mode Fatigue and Fracturre, ESIS 14 (Edited by H.P. Rossmanith and K.J. Miller), Mechanical Engineering Publications, London, pp. 185-199,1993

43. Zheng, X.J., Metzger, D.R., Dubery, R.N., and Glinka, G., Strain Energy Release rate Criterion for Mixed Mode and Interface Cracks- A Numerical Approach, Proc. 15th Canadian Congress of Applied Mechanics, University of Victoria, Victoria, BC, Canada, 1995

44. Hayashi, K. and Nemat-Nasser, S., Energy-Release Rate and Crack Kinking Under Combined Loading, J. Applied Mech., Vol.48, pp. 520-524, 1981

45. Comninou, M., The Interface Crack, ASME J. Applied Mech., Vol. 44, pp 63331-636, 1977

46. Rice, J.R. and Sih, G.C., Plane Problems of Cracks in Dissimilar Media, ASME J. Applied Mech., Vol. 32, pp. 418-423,1965

47. Mukai, D.J., Ballarini, R., and Miller, G.R., Analysis of Branched Interface Cracks, ASME J. Applied Mech., Vol. 57, pp.887-893,1990

48. Wu, K., Stress IntensityFactor and Energy Release Rate for Interfacial Cracks Between Dissimilar Anisotropic Materials, ASME J. Applied Mech, Vol. 57, pp. 882-886, 1990

49. Chen, W., and Keer, L.M., Fatigue Crack Growth in Mixed Mode Loading, ASME J. Applied Mech., Vol. 113, pp.222-227, 1991

50. Reynolds, R.R., Kokini, K., Chen, G., The Mechanics of the Interface Crack Using the Finite Element Method, ASME J. Applied Mech., Vol. 112, pp. 38-43, 1990

51. Ingraffea, A.R., On the Discrete Fracture Propagation in Rocks Loaded in Compression, Proc. Numerical Methods in Fracture Mechanics, pp. 235-248, Swansea, U.K., 1978

52. Henshell, R.D., and Shaw, K.G., Crack Tip Elements are Unnecessary, Int. J. Numer. Meth. Eng., 9, 495-509, 1975

53. Kardestuncer, H., Norrie, D.H., and Brezzi, F. (1987). "Finite element handbook.", McGraw Hill, Inc., 4.138-4.139.

54 ANSYS User's Manual, Swanson Analysis Systems, Inc., Revision 5.0, Vol. IV Theory, 1992.

55. Arora, J.S., Introduction to Optimum Design, McGraw-Hill, Inc., 1989

56. Schittkowski, K "NLPQL: A Fortran subroutine solving constrained nonlinear programming problems", Working Paper, University of Stuttgart (1984).

57. Schittkowski, K., The Nonlinear Programming Method of Wilson, Han, and Powell with an Augmented Lagrangian Type Line Search Function Part 1: Convergence Analysis, Numerische Mathematik, 38, 115-127 (1981).

58. Schittkowski, K., The Nonlinear Programming Method of Wilson, Han, and Powell with an Augmented Lagrangian Type Line Search Function Part 2: An Efficient Implementation with Linear Least Squares Subproblems., Numerische Mathematik, 38, 115-127 (1981).

59. Vaessen, W, Nonlinear Function Optimization, UBC NLP, University of British Columbia Computing Centre, 1984.

60. Schittkowski, K., Test Examples for Nonlinear Programming Codes, Lecture Notes in Econ. & Math, 1981.

61. Schittkowski, K., More Test Examples for Nonlinear Programming Codes, Lecture Notes in Econ. & Math, 1987.

62. Thanedar, P.B., Arora, J.S., Tseng, C.H., Lim, O.K., Park, G.L., Performance of Some SQP Algorithms on Structural Design Problems, International Journel for Numerical Methods in Engineering, Vol. 23, 2187-2203, 1986.

63. Broek, D., Elementary Engineering Fracture Mechanics, Fourth revised edition, Kluwer Acedemic publishers, Dordrecht, 1986

64. ANSYS User's Manual, Swanson Analysis Systems, Inc., Revision 5.0, Vol I Procedure, 1992.

65. Polis, M.P., The distributed system parameter identification problem: a survey of recent results, Proc. of 3rd IFAC Symp. on Control of Distrubuted Parameter Systems, pp. 45-58, Pergamon Press, Oxford, 1982

66. Fadale, T.D., Nenarokomov, A.V., and Emery, A.F., Uncertainties in parameter estimation: the inverse problem, Int. J. Heat and Mass Transfer, Vol.38, No. 3, pp. 511-518, 1995.

67. Bratley, P. and Fox, B.L., ALGORITHM 659 Implementing Sobol's Quasirandom Sequence Generator, ACM Trans. on Mathematical Software, Vol. 14, No. 1, pp. 88-100,1988.

68. Hull, D., An Introduction to Composite Materials, Cambridge University Press, 1981

69. Roger, G., Mechanics of Engineering Structures, Wiley, New York, 1962.